Supporting Information

Rim-Brominated Pillarplexes and their Assembly via Self-Sorting

Julian Zuber,[a] Thomas Pickl,[a] Alexandra A. Heidecker,[a] Marco Baron,[b] Christian Jandl[c] and Alexander Pöthig[*a]

[a.] Catalysis Research Center & Department of Chemistry, Technische Universität München, Ernst-Otto-Fischer-Str. 1, 85747 Garching bei München, Germany

[b.] Dipartimento di Scienze Chimiche, Università degli Studi di Padova, via Marzolo 1, 35131 Padova, Italy

[c.] ELDICO Scientific AG Switzerland Innovation Park Basel Area, Hegenheimermattweg 167A, 4123 Allschwil, Switzerland

[*]**Corresponding Author**

Email: **alexander.poethig@tum.de**

Table of Contents

Supporting Information **1**

1. General Remarks **3**

2. Experimental details **3**

3. NMR spectra of compound $H_6L^{Br2}(OTf)_4$ **6**

4. NMR spectra of compound $H_6L^{Br2}(PF_6)_4$ **8**

5. NMR spectra of compound $Ag_8(L^{Br2})_2(PF_6)_4$ **11**

6. NMR spectra of compound $Au_8(L^{Br2})_2(PF_6)_4$ **14**

7. VT NMR spectra **16**

8. HRESI-MS spectra **20**

8.1 HRESI-MS spectrum of $H_6L^{Br2}(OTf)_4$ 20

8.2 HRESI-MS spectrum of $H_6L^{Br2}(PF_6)_4$ 21

8.3 HRESI-MS spectrum of $Ag_8(L^{Br2})_2(PF_6)_4$ 22

8.4 HRESI-MS spectrum of $Au_8(L^{Br2})_2(PF_6)_4$ 24

9. Self-Sorting Experiments **25**

9.1 HRESI-MS Studies 25

9.2 NMR Studies 30

10. Computational Methods **37**

11. Electron Diffraction **40**

11.1 Compound $H_6L^{Br2}(OTf)_4$ (2374511) 40

12. Crystallographic details **42**

12.1 Compound $H_6L^{Br2}(PF_6)_4$ (2374510) 42

12.2 Compound $Ag_8(L^{Br2})_2(PF_6)_4$ (2374512) 44

12.3 Compound $Au_8(L^{Br2})_2(PF_6)_4$ (2374513) 47

13. References **51**

1. General Remarks

All commercially available chemicals were purchased at *abcr*, *Acros Organics*, *Alfa Aesar*, *Carbolution Chemicals*, *Merck* or *Sigma-Aldrich* and used without further purification unless stated otherwise. Compounds which are commercially unavailable were prepared according to the literature-known procedures. Experiments including air and moisture sensitive compounds were carried out under standard Schlenk techniques in preheated glassware using argon 4.6 from *Westfalen* or in a UNIlab glovebox from *MBraun*. All syringes, magnetic stirring bars and needles were rigorously dried. Dry solvents were obtained from an *MBraun* solvent purification system (SPS) and were used without further purification. Technical solvents were distilled prior to use (CH_2Cl_2, $CHCl_3$, MeCN, MeOH, EtOH, Et_2O, pentane and hexane). The deuterated solvent (MeCN-d_3) was stored over activated 4 Å molecular sieves.

NMR Spectroscopy

NMR spectra were recorded at room temperature (293–298 K) on *Bruker* AV-400US, DRX 400, AVHD-400, AVHD-500 or AV-500C spectrometers. The spectra were processed using *MestReNova* 14.2.0. All chemical shifts (δ) are given in *parts per million* (ppm).The scalar coupling constants ^nJ are given in *Hertz* (Hz). For signal multiplicities, the following abbreviations were used: s = singlet, d = doublet, t = triplet, q = quartet, quint = quintet, sept = septet, m = multiplet, br = broad and combinations thereof. ^{1}H NMR spectra were referenced to the residual proton signals of MeCN-d_3 (δ = 1.94 ppm) with respect to Me_4Si (δ = 7.26 ppm). ^{13}C NMR spectra were referenced to the ^{13}C-D septet of MeCN-d_3 (δ = 1.32 ppm). ^{19}F NMR spectra with ^{1}H-decoupling were recorded at AVHD-400. Correlation NMR experiments like ^{1}H-^{1}H COSY, ^{1}H-^{13}C HSQC and ^{1}H-^{13}C HMBC were used to assign the ^{1}H and ^{13}C NMR signals.

HRESI-MS

Analysis of HRESI-MS was carried out on a *Thermo Fisher* Exactive Plus Orbitrap mass spectrometer with a *Thermo Fisher* ESI source. Samples were prepared as 50 µg mL^{-1} solutions in acetonitrile, syringe filtered to 22 µm and injected with an ionisation voltage of 3.80 kV while ions were detected in the positive mode. Peaks were fit with Gaussian functions and compared to isotope patterns calculated by *enviPat* Web 2.6.[1] Mass-charge ratios *m/z* are given in g mol^{-1} e^{-1}.

2. Experimental details

Calix[4]imidazolium[2]dibromo-pyrazole tetrakis(triflate) ($H_6L^{Br2}(OTf)_4$)

$H_6L(OTf)_4$ (400.0 mg, 370.1 µmol, 1.0 eq.) was dissolved in MeCN (20 mL) and *N*-bromosuccinimide (138.3 mg, 777.2 µmol, 2.1 eq.) in MeCN (10 mL) was added dropwise over the course of 20 min at room temperature. After stirring for 24 h at 40 °C, the solvent of the yellow solution was removed under reduced pressure and the resulting yellow oil was dissolved in a minimum amount of MeCN (0.5 mL). The crude product was precipitated with diethyl ether (30 mL) and isolated by centrifugation. Subsequently, the yellow solid was washed with ethanol and ethyl acetate (2 x 10 mL) and ultrasonicated between the washing steps in order to guarantee suspension of the solid. Drying in vacuo resulted in 308.0 mg (248.7 µmol, 67.2 %) of a yellowish

solid. ^{1}H NMR (400 MHz, MeCN-d_3): δ [ppm] = 12.33 (s, 2H, NH), 9.05 (s, 4H, NCHN), 7.76 (s, 4H, NCHC), 7.57 (s, 4H, NCHC), 6.47 (s, 4H, CH_2), 5.43 (s, 8H, CH_2). ^{13}C NMR (101 MHz, MeCN-d_3): δ [ppm] = 144.6 (br), 138.4, 125.1, 123.8, 121.7 (q, $^{1}J_{C\text{-}F}$ = 320 Hz),118.1 (MeCN), 96.7, 59.8, 46.7 (br), 43.9 (br). ^{19}F NMR (376 MHz, MeCN-d_3): δ [ppm] = -79.3. HRESI-MS (m/z): calcd. 1088.93 $[H_6L^{Br2}(OTf)_3]^+$, 469.99 $[H_6L^{Br2}(OTf)_2]^{2+}$; found 1088.93 $[H_6L^{Br2}(OTf)_3]^+$, 469.99 $[H_6L^{Br2}(OTf)_2]^{2+}$.

Calix[4]imidazolium[2]dibromo-pyrazole tetrakis(hexafluorophosphate) ($H_6L^{Br2}(PF_6)_4$)

$H_6L(PF_6)_4$ (500.0 mg, 430.3 µmol, 1.0 eq.) was dissolved in MeCN (20 mL) and *N*-bromosuccinimide (175.57 mg, 986.5 µmol, 2.1 eq.) in MeCN (10 mL) was added dropwise over the course of 20 min at room temperature. After stirring for one hour at room temperature, the solvent of the orange solution was removed under reduced pressure and the resulting orange oil was dissolved in a minimum amount of MeCN (0.5 mL). The crude product was precipitated with diethyl ether (40 mL) and isolated by centrifugation. Subsequently, the orange solid was washed with water (3 x 10 mL) and ultrasonicated between the washing steps in order to guarantee suspension of the solid. Drying in vacuo resulted in 416.2 mg (340.5 µmol, 72.5 %) of a yellow solid. ^{1}H NMR (400 MHz, MeCN-d_3): δ [ppm] = 11.86 (s, 2H, NH), 8.85 (s, 4H, NCHN), 7.66 (s, 4H, NCHC), 7.53 (s, 4H, NCHC), 6.42 (s, 4H, CH_2), 5.43 (s, 8H, CH_2). ^{13}C NMR (101 MHz, MeCN-d_3): δ [ppm] = 137.9, 125.1, 124.0, 118.3 (MeCN), 96.8, 59.9. ^{19}F NMR (376 MHz, MeCN-d_3): δ [ppm] = -72.65 (d, $^{1}J_{P\text{-}F}$ = 707.1 Hz). ^{31}P NMR (162 MHz, MeCN-d_3): δ [ppm] = -144.7 (sept, $^{1}J_{P\text{-}F}$ = 707.5 Hz). HRESI-MS (m/z): calcd. 1076.96 $[H_6L^{Br2}(PF_6)_3]^+$, 466.00 $[H_6L^{Br2}(PF_6)_2]^{2+}$; found 1076.96 $[H_6L^{Br2}(PF_6)_3]^+$, 466.00 $[H_6L^{Br2}(PF_6)_2]^{2+}$.

Bis(calix[4]imidazolium[2]dibromo-pyrazolato)octakissilver(I)tetrakis(hexafluorophosphate) ($Ag_8(L^{Br2})_2(PF_6)_4$)

$H_6L^{Br2}(PF_6)_4$ (300.0 mg, 245.5 µmol, 1.0 eq.) and Ag_2O (284.4 mg, 1.23 mmol, 5.0 eq.) were dissolved in MeCN (30 mL) in a 50 mL flask. The black suspension was stirred under exclusion of light at room temperature for 16 h and filtered through Celite®. After removing the solvent under reduced pressure, the brown precipitate was dissolved in MeCN (30 mL) and transferred into a big Schlenk tube. Diethyl ether (22 mL) was added until a brown precipitate and a colourless supernatant formed. The mixture was filtered again through Celite® and to the filtrate diethyl ether (170 mL) was added. In order to guarantee complete precipitation, the suspension was stirred under exclusion of light at room temperature for one hour. The precipitate was allowed to settle down, transferred into a conical tube and isolated by centrifugation. Washing with diethyl ether (3 x 10 mL) and drying in vacuo resulted in 311.1 mg (114.6 µmol, 93.4 %) of a white solid. ^{1}H NMR (400 MHz, MeCN-d_3): δ [ppm] = 7.62 (d, ^{3}J = 2.1 Hz, 8H, NCHC), 7.60 (d, ^{3}J = 2.1 Hz, 8H, NCHC), 6.59 (d, ^{2}J = 14.7 Hz, 4H, CH_2), 6.08 (d, ^{2}J = 14.9 Hz, 4H, CH_2), 5.66 (d, ^{2}J = 15.4 Hz, 8H, CH_2), 5.23 (d, ^{2}J = 15.4 Hz, 8H, CH_2). ^{13}C NMR (101 MHz, MeCN-d_3): δ [ppm] = 178.0, 148.3, 125.7, 123.1, 118.3 (MeCN), 94.9, 65.6, 48.0. ^{19}F NMR (376 MHz, MeCN-d_3): δ [ppm] = -72.70 (d, $^{1}J_{P\text{-}F}$ = 707.1 Hz). ^{31}P NMR (162 MHz, MeCN-d_3): δ [ppm] = -142.4 (sept, $^{1}J_{P\text{-}F}$ = 707.2 Hz). HRESI-MS (m/z): calcd. 1212.61 $[Ag_8(L^{Br2})_2(PF_6)_2]^{2+}$, 760.09 $[Ag_8(L^{Br2})_2(PF_6)]^{3+}$, 533.82 $[Ag_8(L^{Br2})_2]^{4+}$; found 1212.61 $[Ag_8(L^{Br2})_2(PF_6)_2]^{2+}$, 760.08 $[Ag_8(L^{Br2})_2(PF_6)]^{3+}$, 533.82 $[Ag_8(L^{Br2})_2]^{4+}$.

Bis(calix[4]imidazolium[2]dibromo-pyrazolato)octakisgold(I)tetrakis(hexafluorophosphate) ($Au_8(L^{Br2})_2(PF_6)_4$)

$Ag_8(L^{Br2})_2(PF_6)_4$ (200.0 mg, 73.65 µmol, 1.0 eq.) in MeCN (10 mL) was added to a stirred solution of Au(THT)Cl (200.7, 626.05 µmol, 8.5 eq.) in MeCN (5 mL) dropwise over the course of 20 min under exclusion of light. The yellow solution was stirred under the exclusion of light at 40 °C for 16 h and the crude product was filtered through Celite® after adding approximately 1 eq. of diethyl ether (5 mL). After precipitating the filtrate with diethyl ether (150 mL) and stirring under exclusion of light at room temperature for one hour, the precipitate was allowed to settle down and the solvents were decanted. The residual suspension was transferred into a conical tube, the solid isolated by centrifugation and washed with DCM (1 x 5 mL). Drying in vacuo resulted in 233.0 mg (67.97 µmol, 92.3 %) of a white solid. ^{1}H NMR (400 MHz, MeCN-d_3): δ [ppm] = 7.69 (s, 16H, NCHC), 6.93 (d, ^2J = 15.0 Hz, 4H, CH_2), 5.98 (d, ^2J = 15.0 Hz, 4H, CH_2), 5.75 (d, ^2J = 15.4 Hz, 8H, CH_2), 5.27 (d, ^2J = 15.4 Hz, 8H, CH_2). ^{13}C NMR (101 MHz, MeCN-d_3): δ [ppm] = 168.6, 147.3, 125.5, 123.9, 118.3 (MeCN), 97.6, 64.3, 47.3. ^{19}F NMR (376 MHz, MeCN-d_3): δ [ppm] = -72.78 (d, $^1J_{P\text{-}F}$ = 706.4 Hz). HRESI-MS (m/z): calcd. 1568.86 $[Au_8(L^{Br2})_2(PF_6)_2]^{2+}$, 997.58 $[Au_8(L^{Br2})_2(PF_6)]^{3+}$, 711.9466 $[Au_8(L^{Br2})_2]^{4+}$; found 1568.85 $[Au_8(L^{Br2})_2(PF_6)_2]^{2+}$, 997.58 $[Au_8(L^{Br2})_2(PF_6)]^{3+}$, 711.94 $[Au_8(L^{Br2})_2]^{4+}$.

3. NMR spectra of compound $H_6L^{Br2}(OTf)_4$

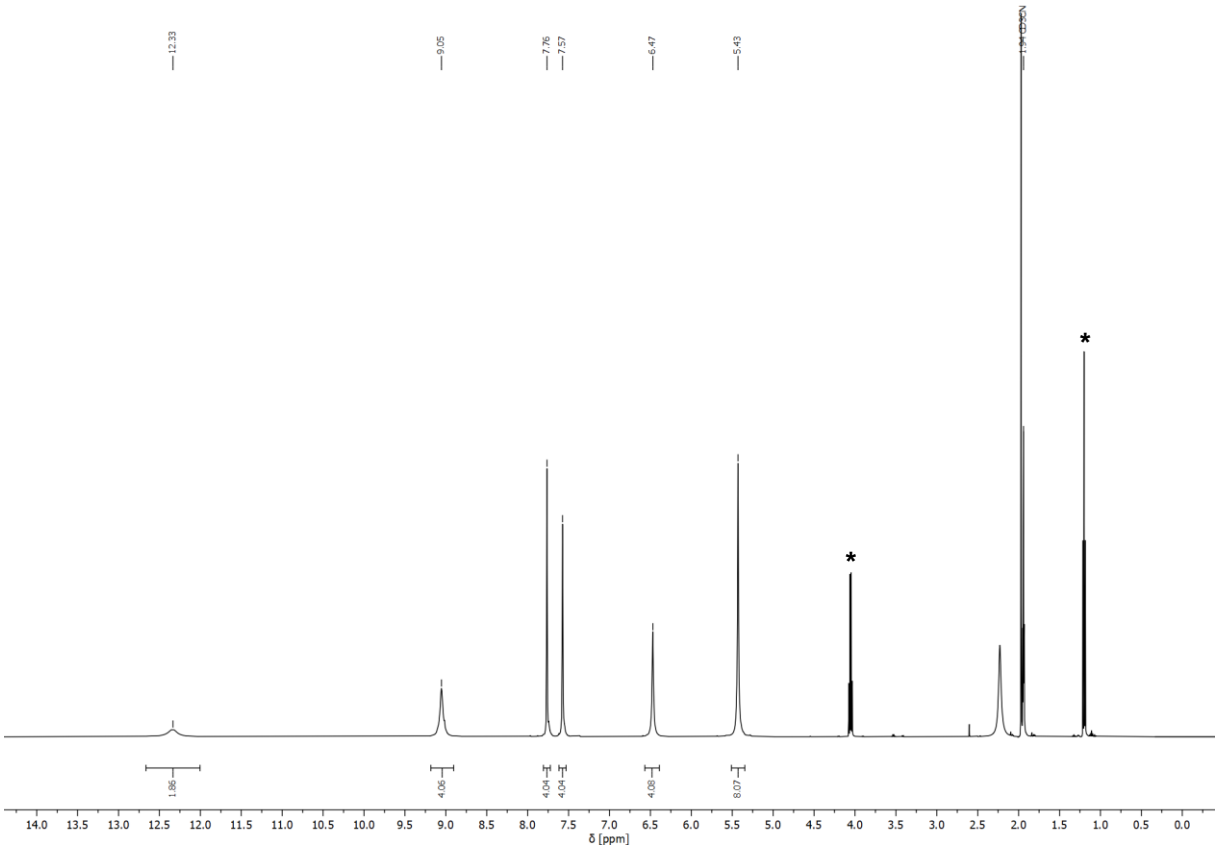

Figure S1: ^{1}H NMR spectrum of $H_6L^{Br2}(OTf)_4$ in MeCN-d_3 at 400 MHz. The signals marked by * are attributed to EtOAc.

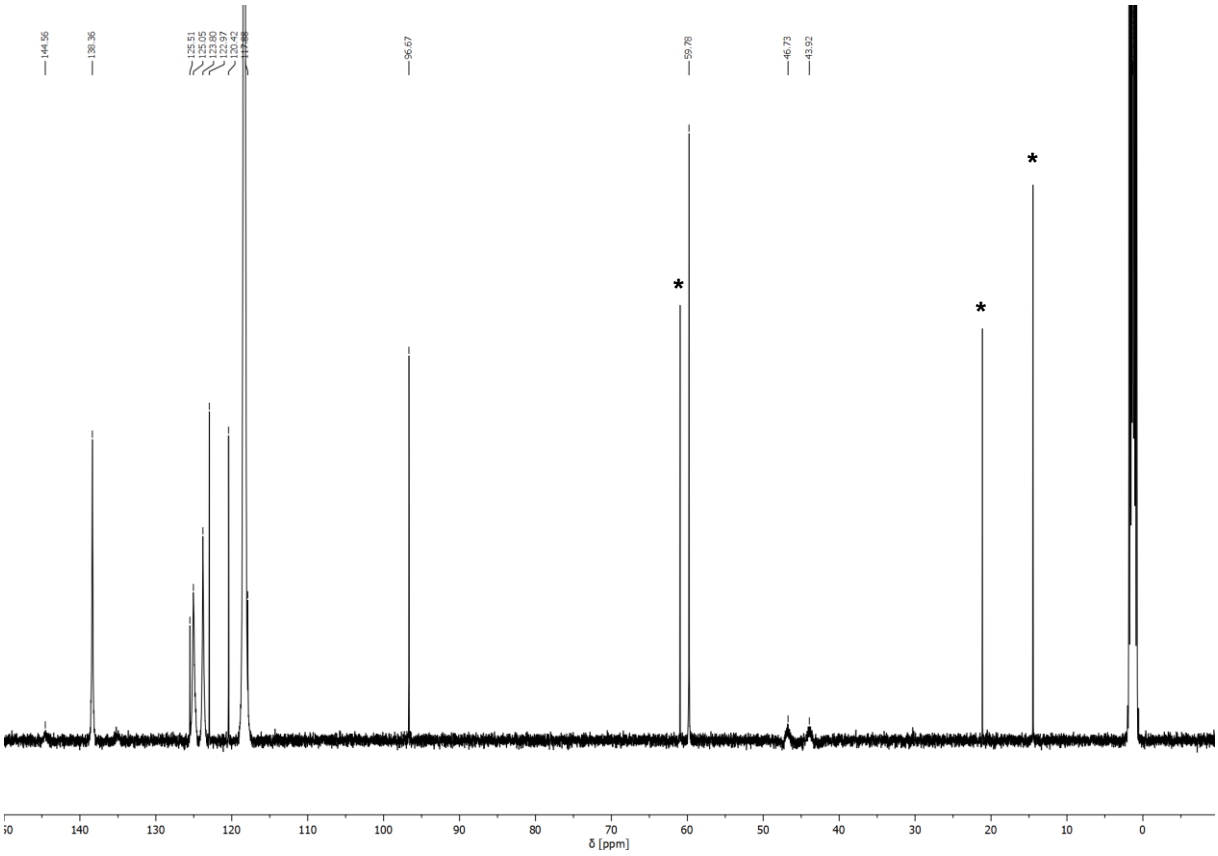

Figure S2: ^{13}C NMR spectrum of $H_6L^{Br2}(OTf)_4$ in MeCN-d_3 at 101 MHz. The signals marked by * are attributed to EtOAc.

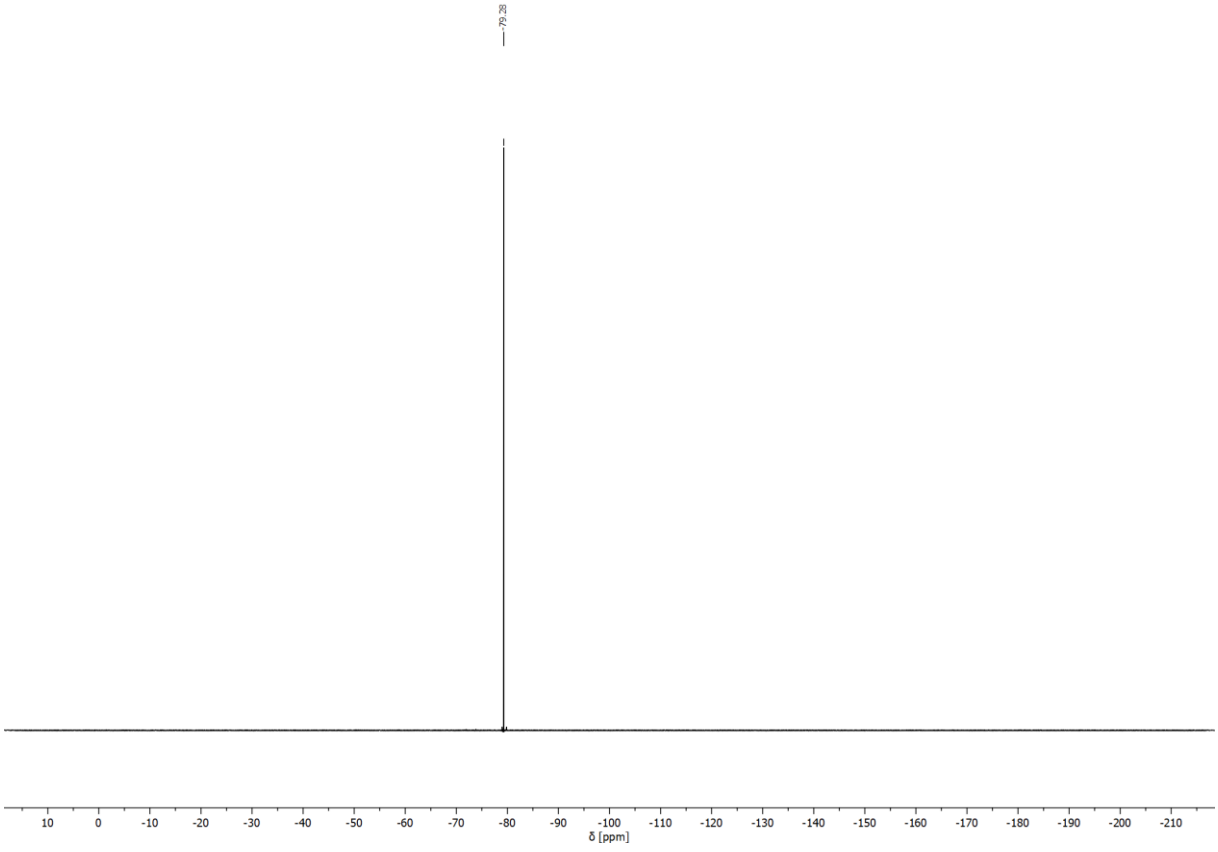

Figure S3: ^{19}F NMR spectrum of $H_6L^{Br2}(OTf)_4$ in MeCN-d_3 at 376 MHz.

4. NMR spectra of compound $H_6L^{Br2}(PF_6)_4$

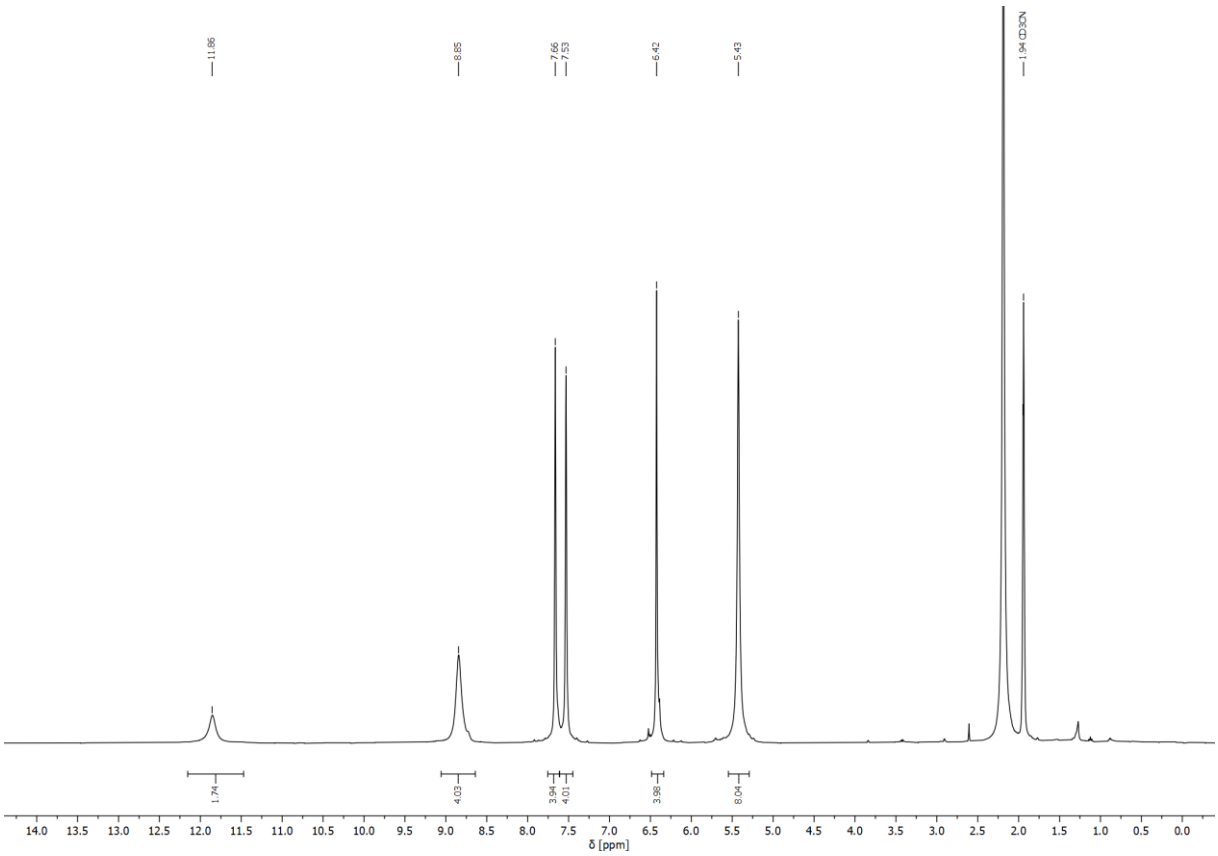

Figure S4: ^{1}H NMR spectrum of $H_6L^{Br2}(PF_6)_4$ in MeCN-d_3 at 400 MHz.

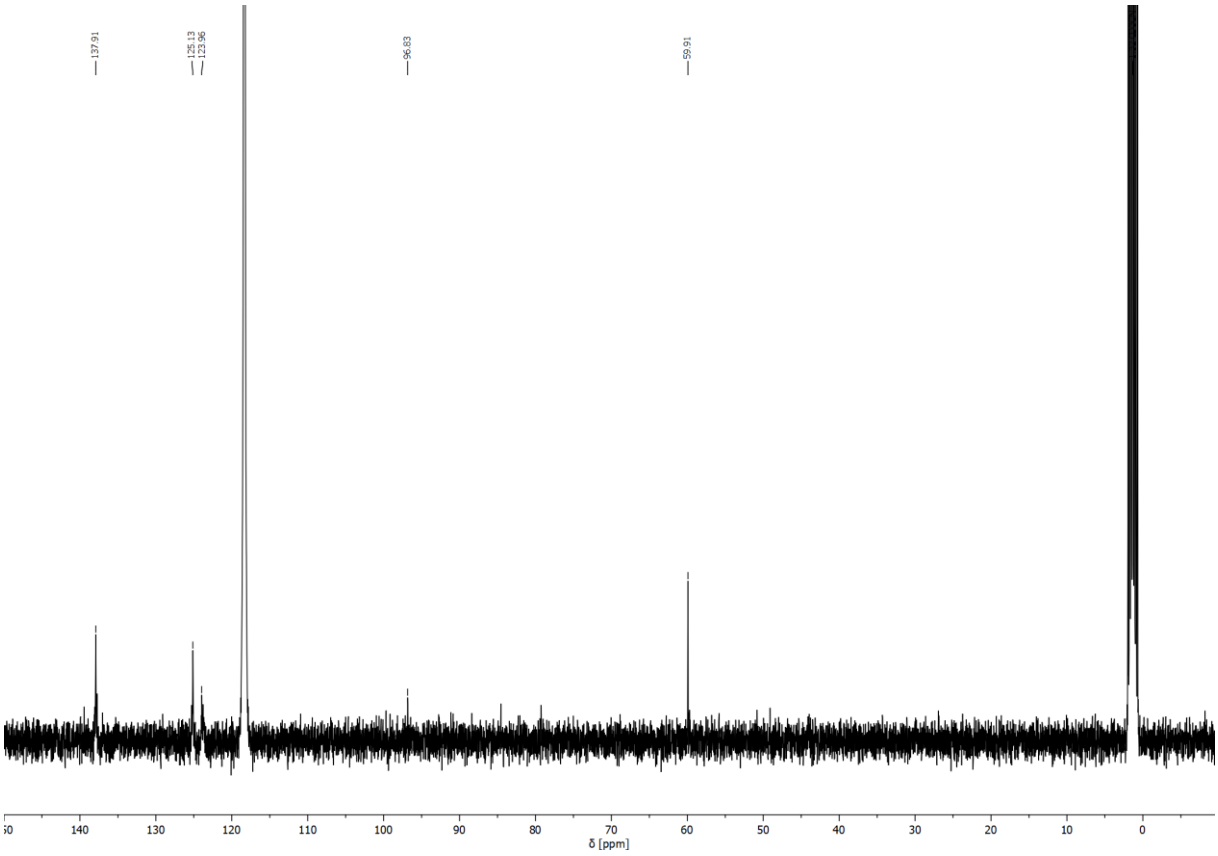

Figure S5: ^{13}C NMR spectrum of $H_6L^{Br2}(PF_6)_4$ in MeCN-d_3 at 101 MHz.

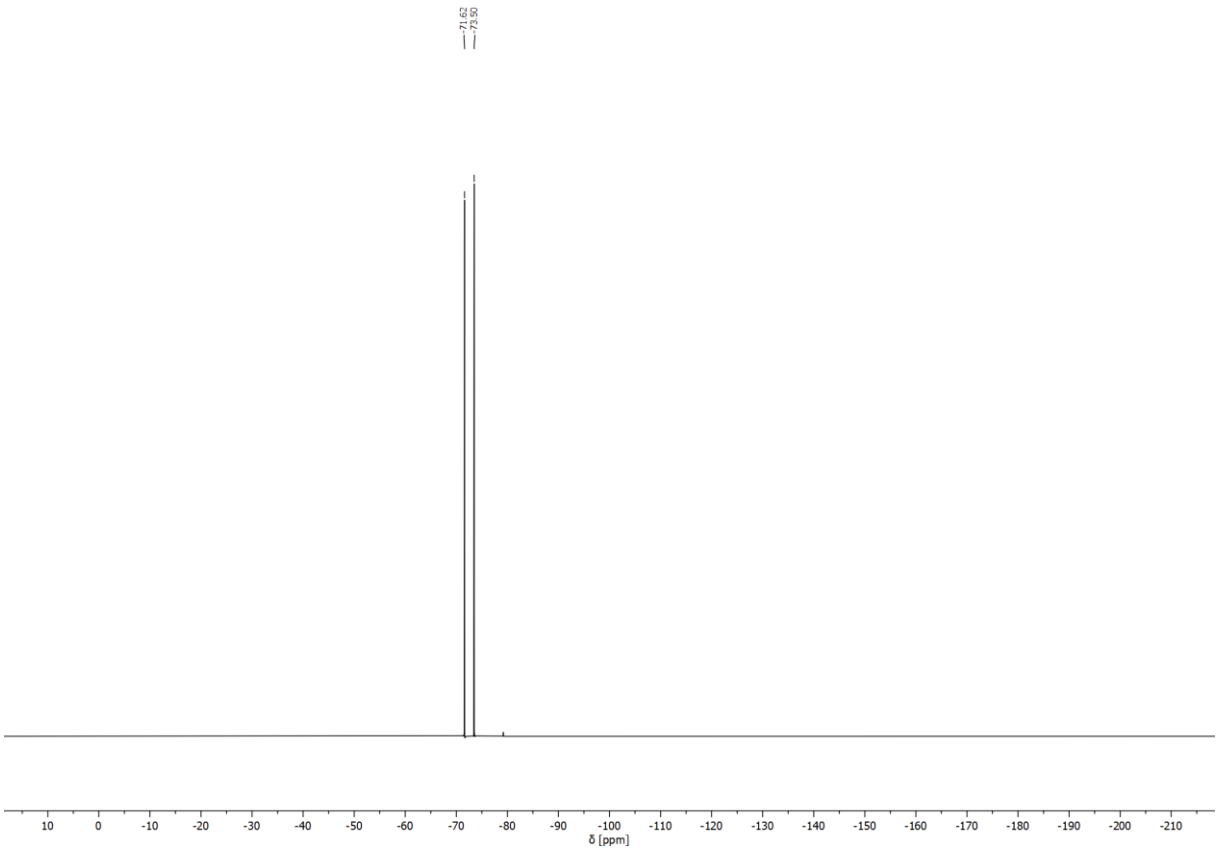

Figure S6: ^{19}F NMR spectrum of $H_6L^{Br2}(PF_6)_4$ in MeCN-d_3 at 376 MHz.

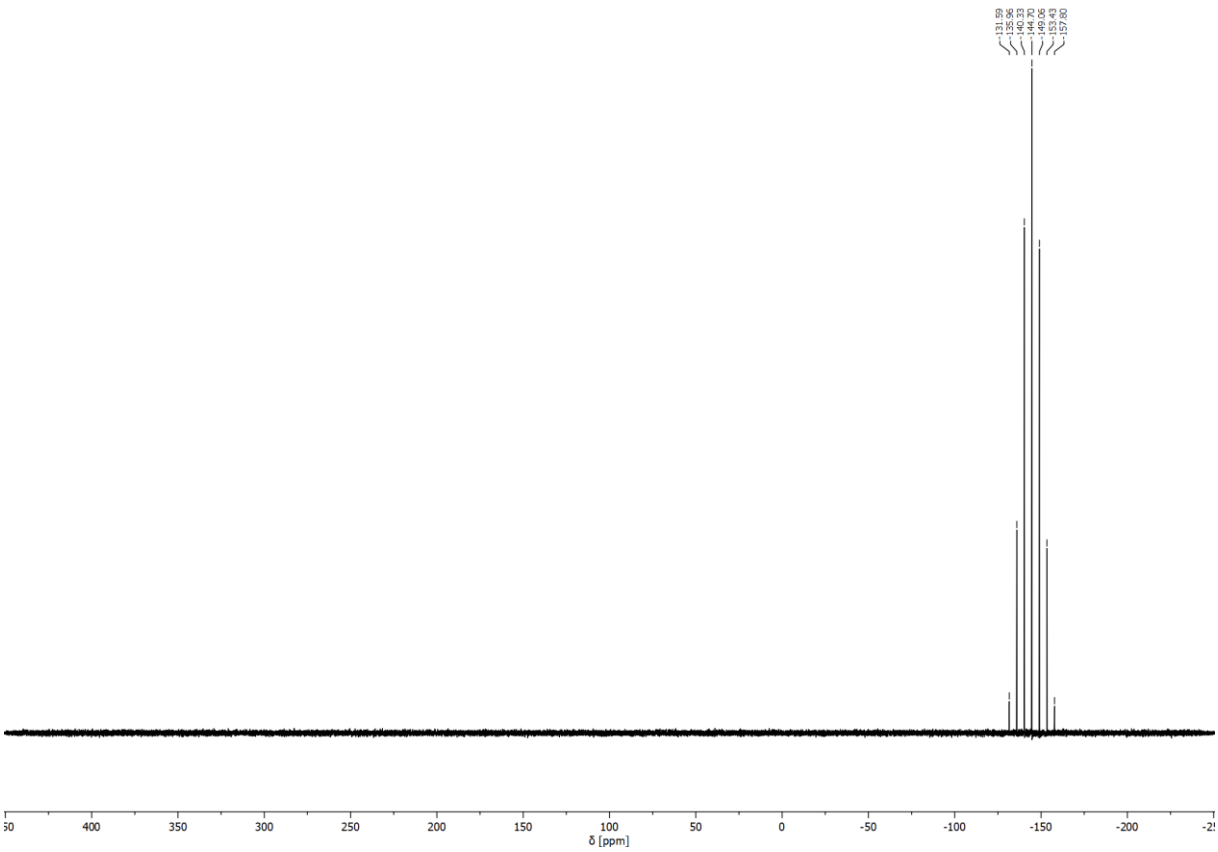

Figure S7: ^{31}P NMR spectrum of $H_6L^{Br2}(PF_6)_4$ in MeCN-d_3 at 162 MHz.

5. NMR spectra of compound $Ag_8(L^{Br2})_2(PF_6)_4$

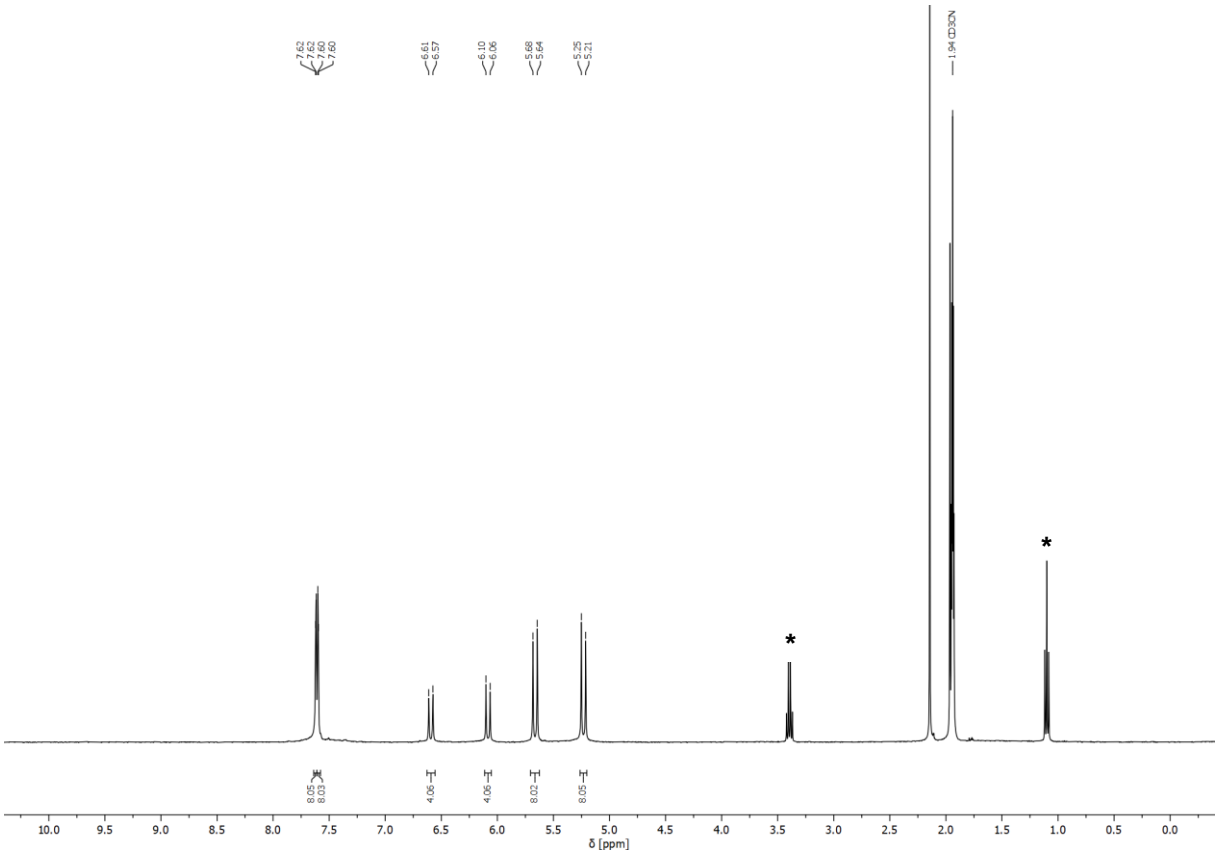

Figure S8: ^{1}H NMR spectrum of $Ag_8(L^{Br2})_2(PF_6)_4$ in MeCN-d_3 at 400 MHz. The signals marked by * are attributed to Et_2O.

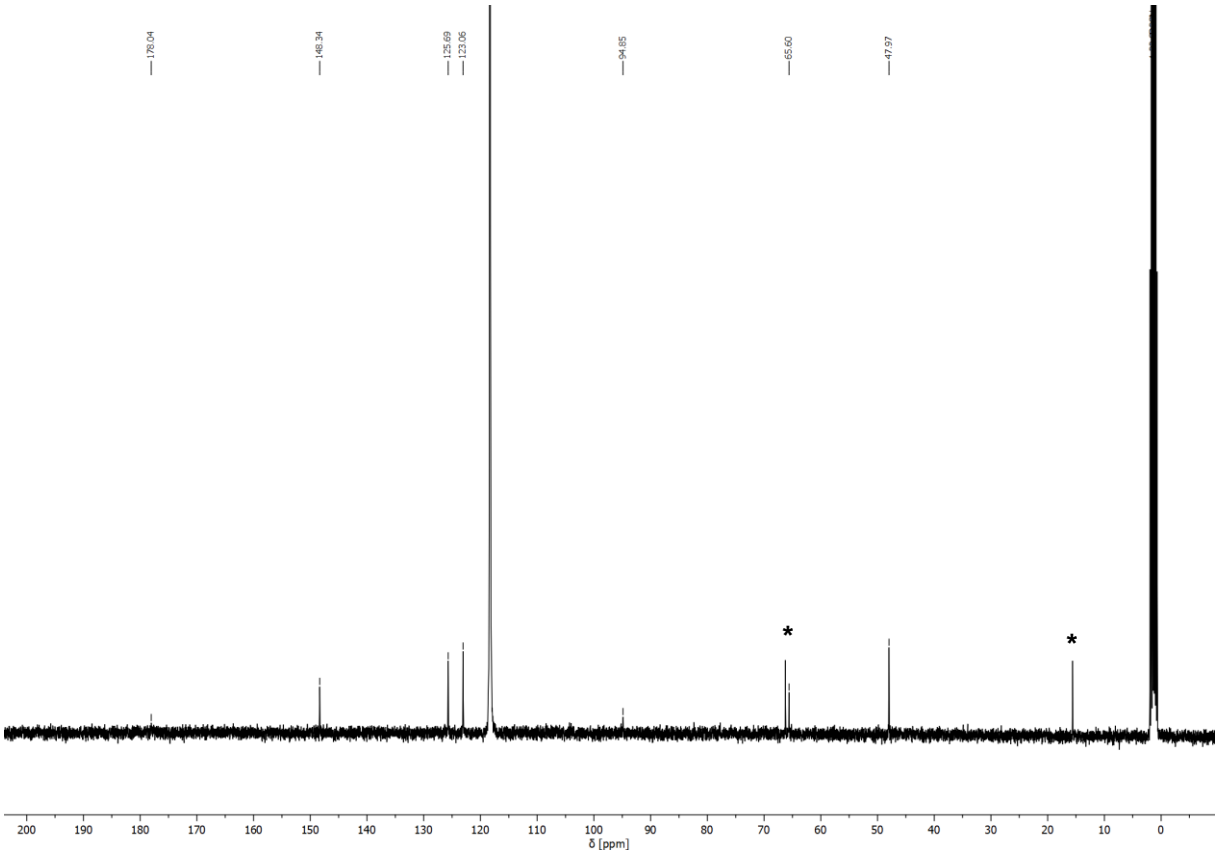

Figure S9: ^{13}C NMR spectrum of $Ag_8(L^{Br2})_2(PF_6)_4$ in MeCN-d_3 at 101 MHz. The signals marked by * are attributed to Et_2O.

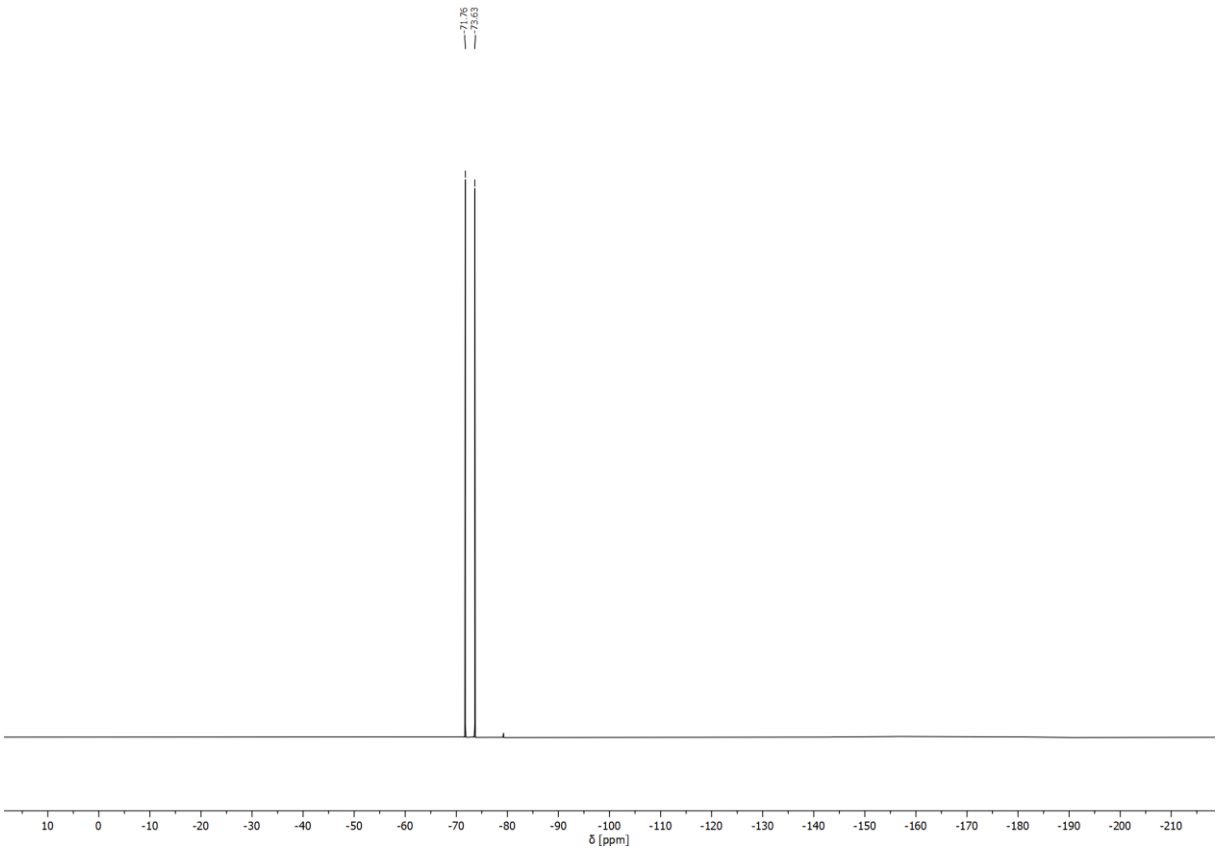

Figure S10: ^{19}F NMR spectrum of $Ag_8(L^{Br2})_2(PF_6)_4$ in MeCN-d_3 at 376 MHz.

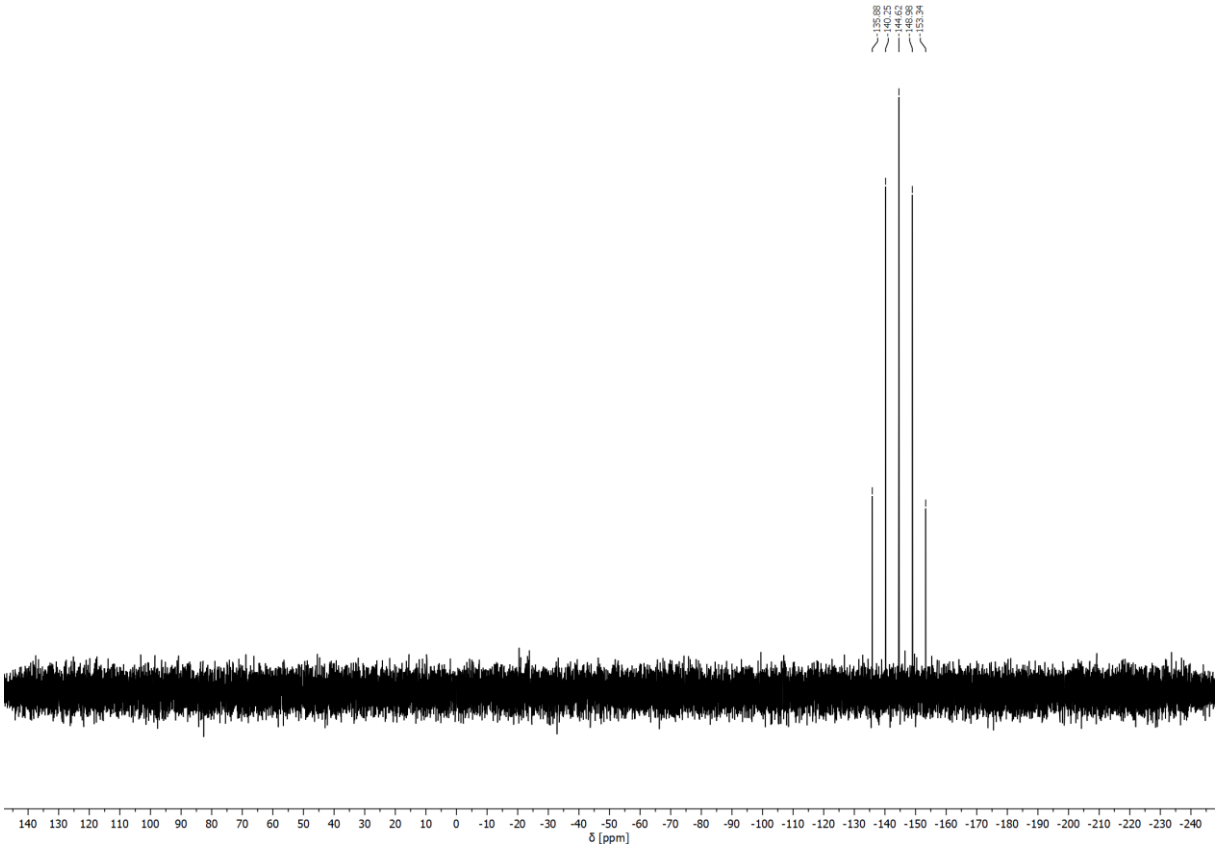

Figure S11: ^{31}P NMR spectrum of $Ag_8(L^{Br2})_2(PF_6)_4$ in MeCN-d_3 at 162 MHz.

6. NMR spectra of compound $Au_8(L^{Br2})_2(PF_6)_4$

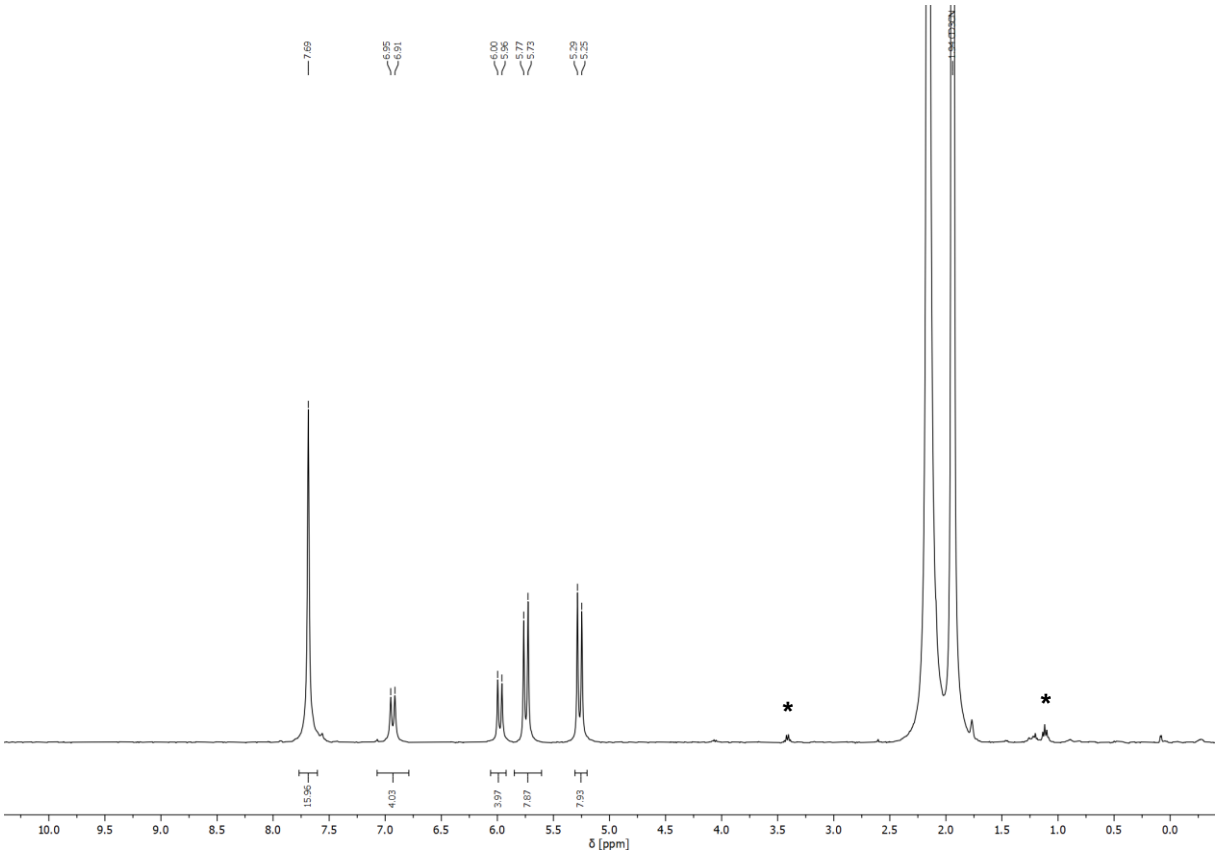

Figure S12: ^{1}H NMR spectrum of $Au_8(L^{Br2})_2(PF_6)_4$ in MeCN-d_3 at 400 MHz. The signals marked by * are attributed to Et_2O.

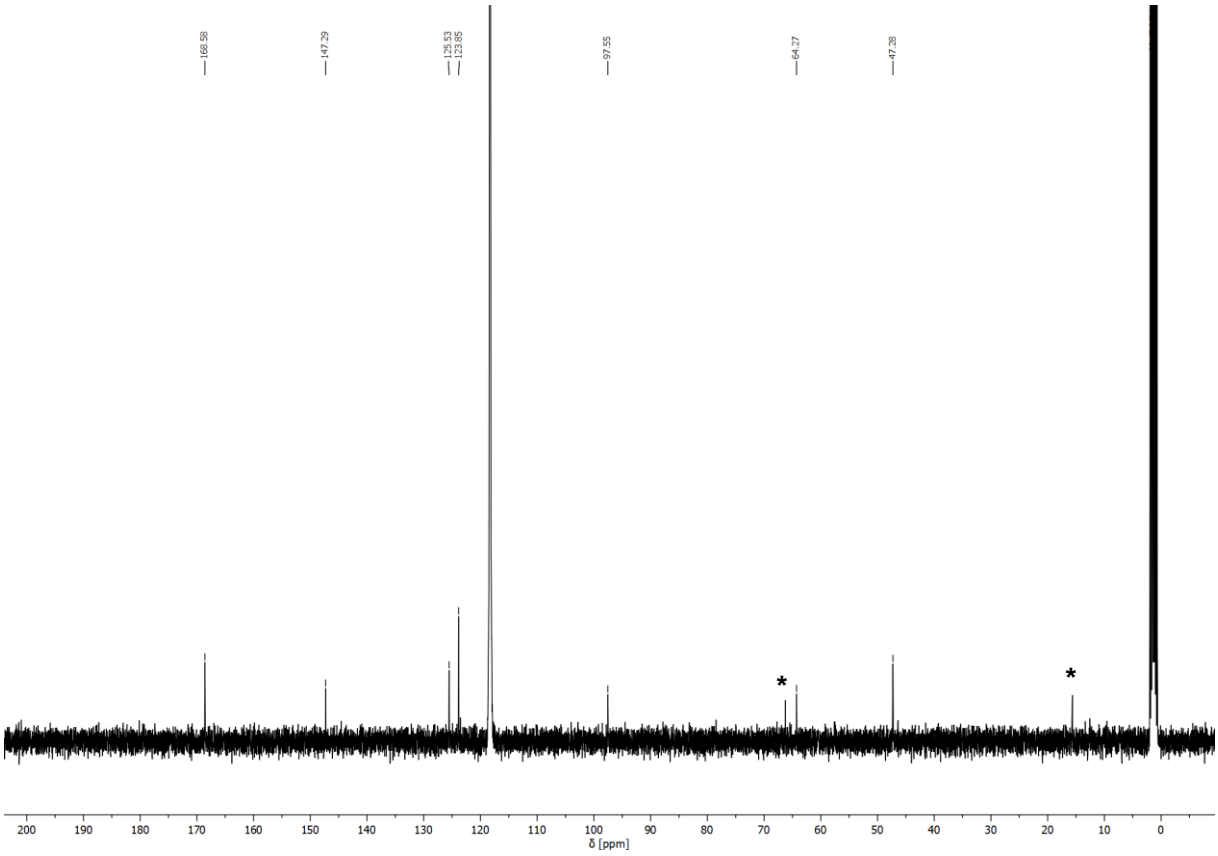

Figure S13: ^{13}C NMR spectrum of $Au_8(L^{Br2})_2(PF_6)_4$ in MeCN-d_3 at 101 MHz. The signals marked by * are attributed to Et_2O.

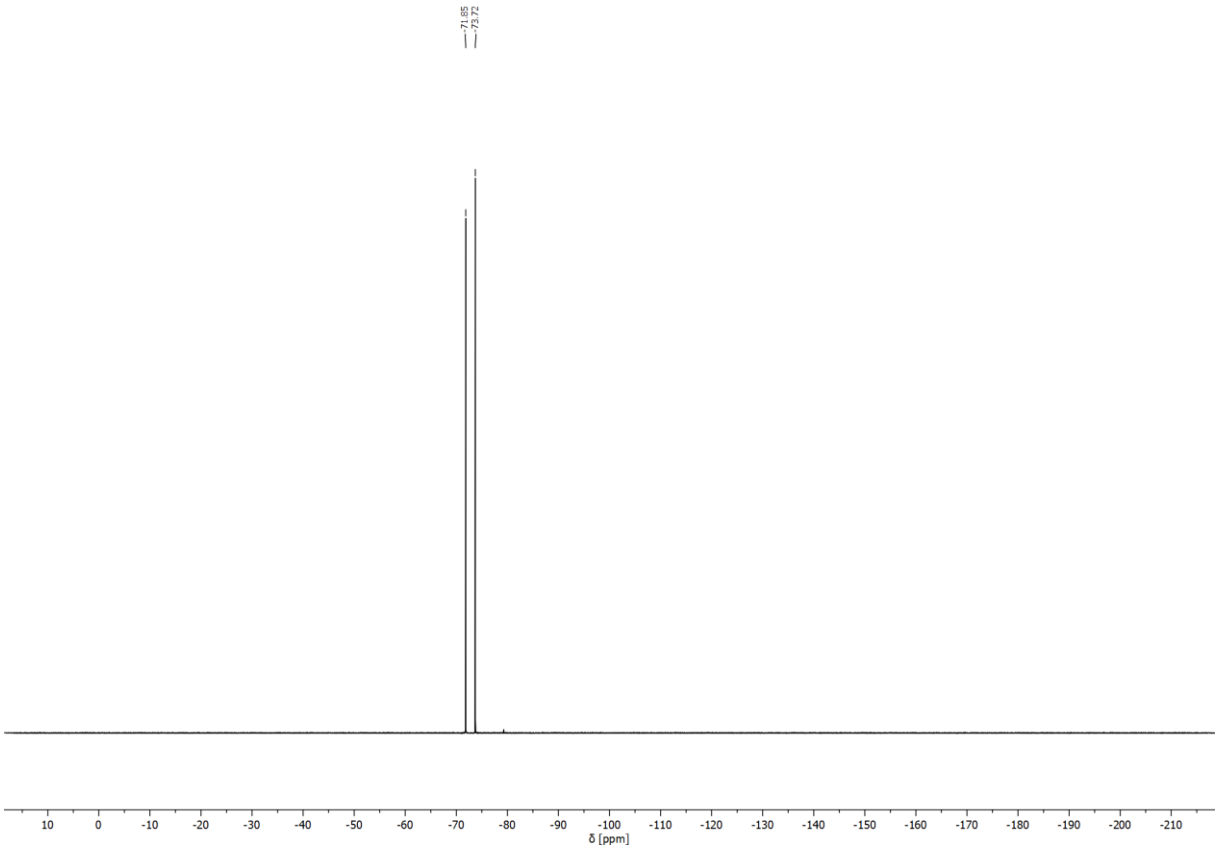

Figure S14: ^{19}F NMR spectrum of $Au_8(L^{Br2})_2(PF_6)_4$ in MeCN-d_3 at 376 MHz.

7. VT NMR spectra

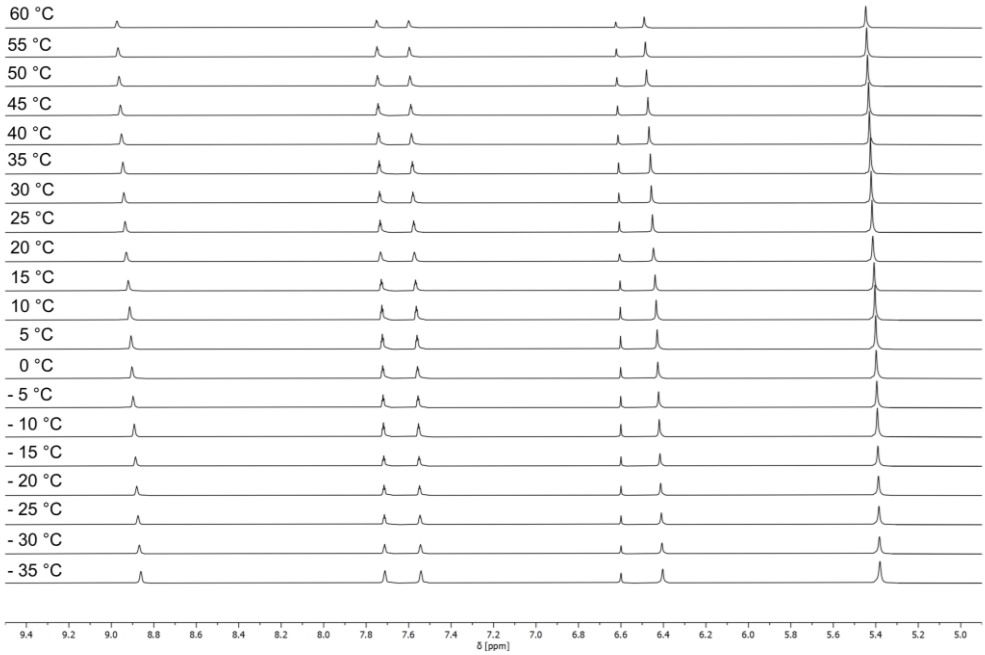

Figure S15: ^{1}H VT-NMR spectrum of $H_6L(OTf)_4$ in MeCN-d_3 at 400 MHz.

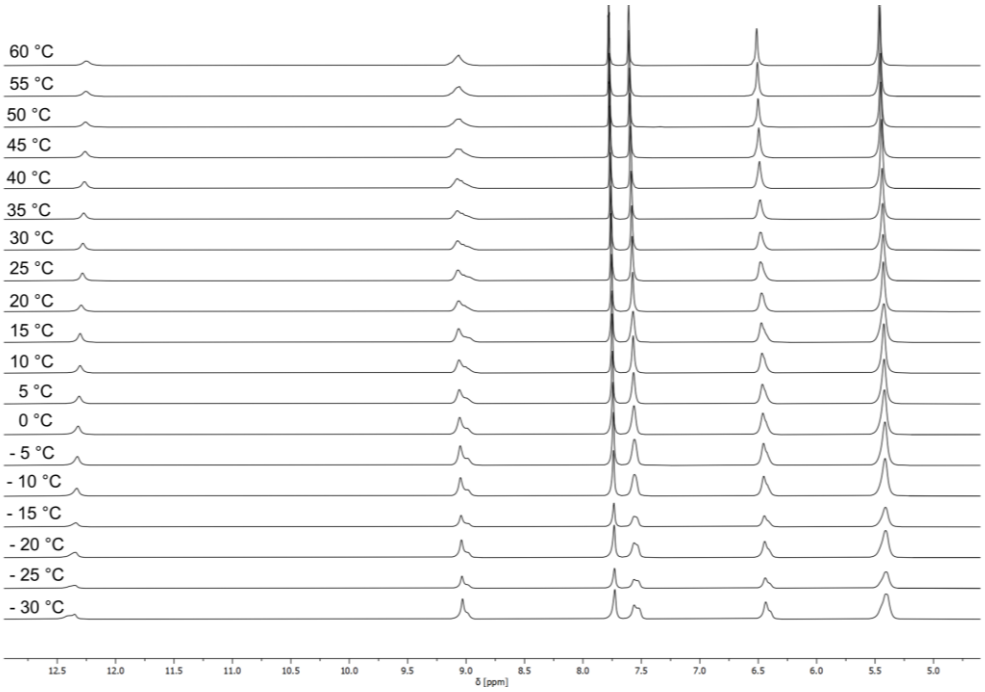

Figure S16: ^{1}H VT-NMR spectrum of $H_6L^{Br2}(OTf)_4$ in MeCN-d_3 at 400 MHz.

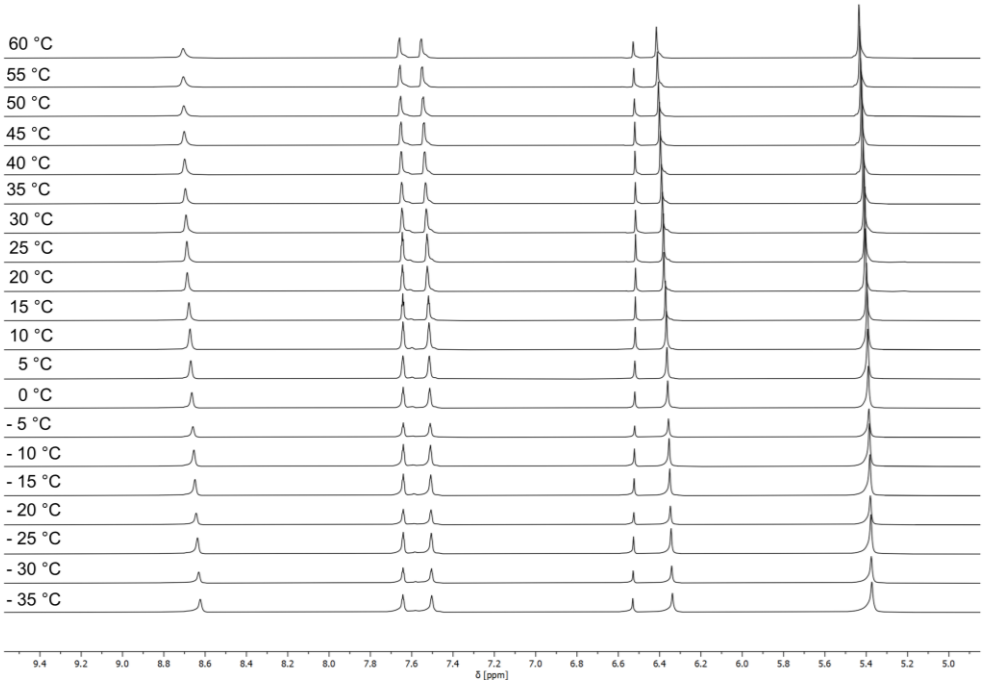

Figure S17: ^{1}H VT-NMR spectrum of $H_6L(PF_6)_4$ in MeCN-d_3 at 400 MHz.

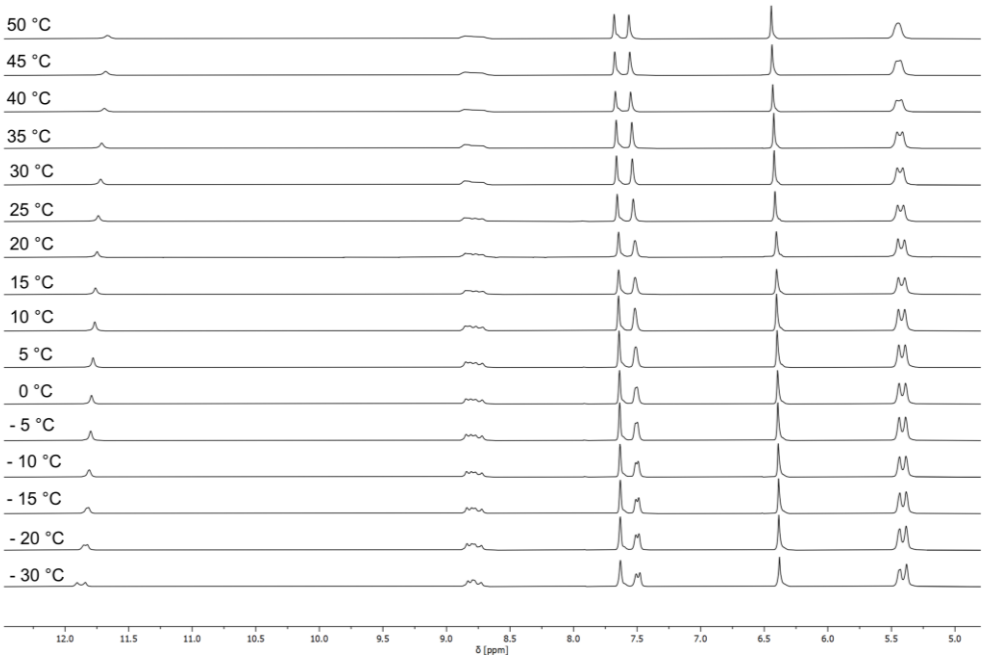

Figure S18: ^{1}H VT-NMR spectrum of $H_6L^{Br2}(PF_6)_4$ in MeCN-d_3 at 400 MHz.

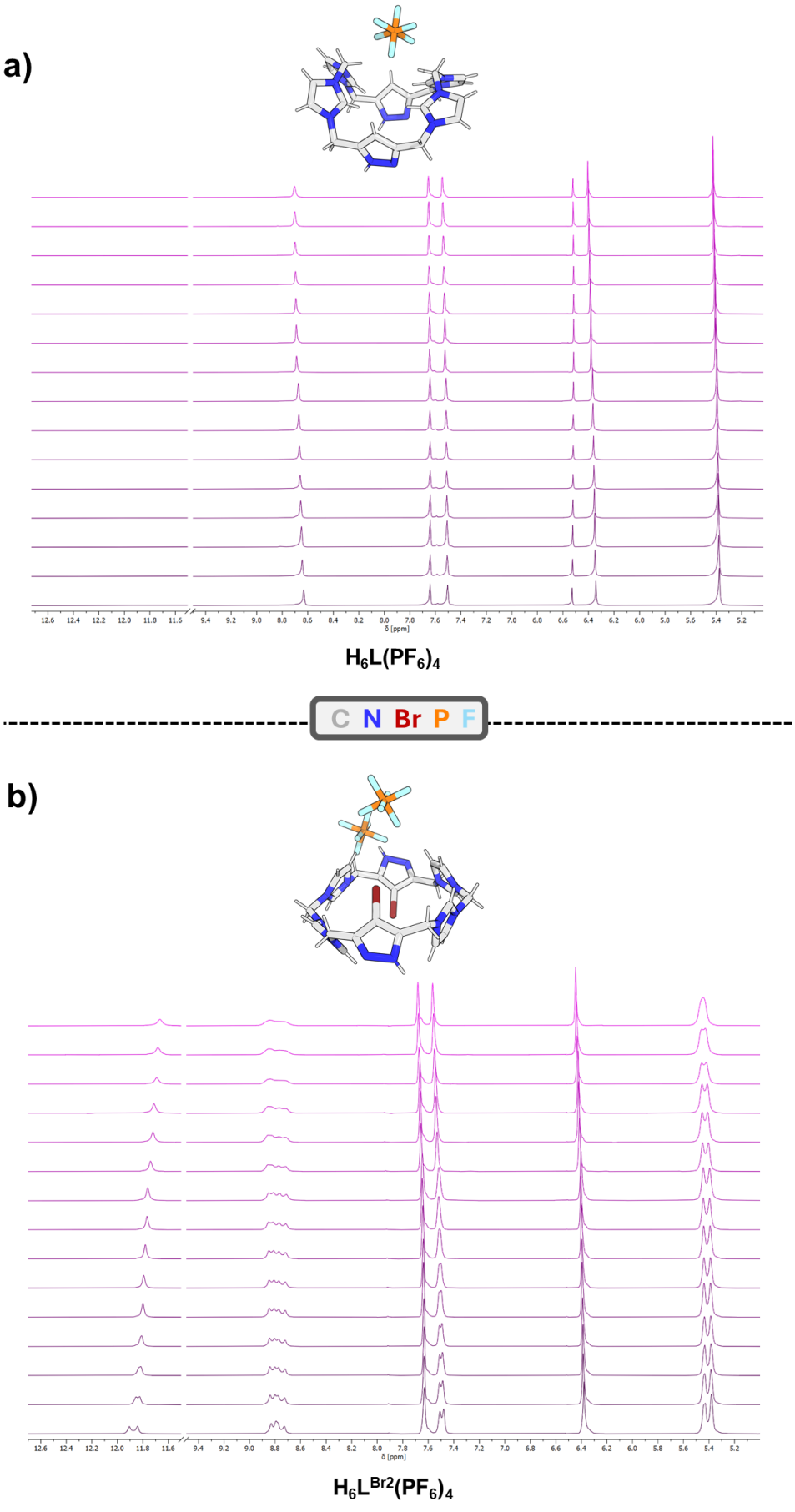

Figure S19: ^{1}H VT-NMR experiments of a) $H_6L(PF_6)_4$ and b) $H6L^{Br2}(PF_6)_4$ in MeCN-d_3 varying from -30 °C to 50 °C.

Table S1: Coalescence temperatures of $H_6L(PF_6)_4$ and $H_6L^{Br2}(PF_6)_4$ in MeCN-d_3.

Proton	$H_6L(PF_6)_4$ [°C]	$H_6L^{Br2}(PF_6)_4$ [°C]
NH	-	-10
NCHN	< -35	> 50
NCHC	40	< -30
NCHC	40	0
CCHC	< -35	-
CH_2	< -35	< -30
CH_2	< -35	50

8. HRESI-MS spectra

8.1 HRESI-MS spectrum of $H_6L^{Br2}(OTf)_4$

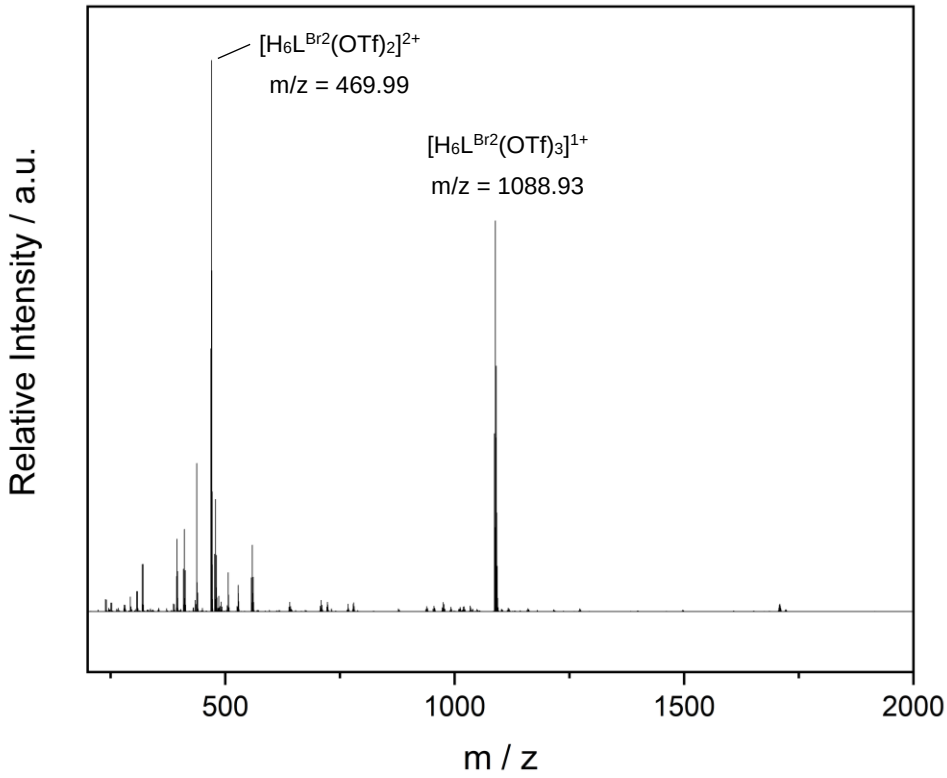

Figure S20: HRESI-MS spectrum of $H_6L^{Br2}(OTf)_4$ in MeCN.

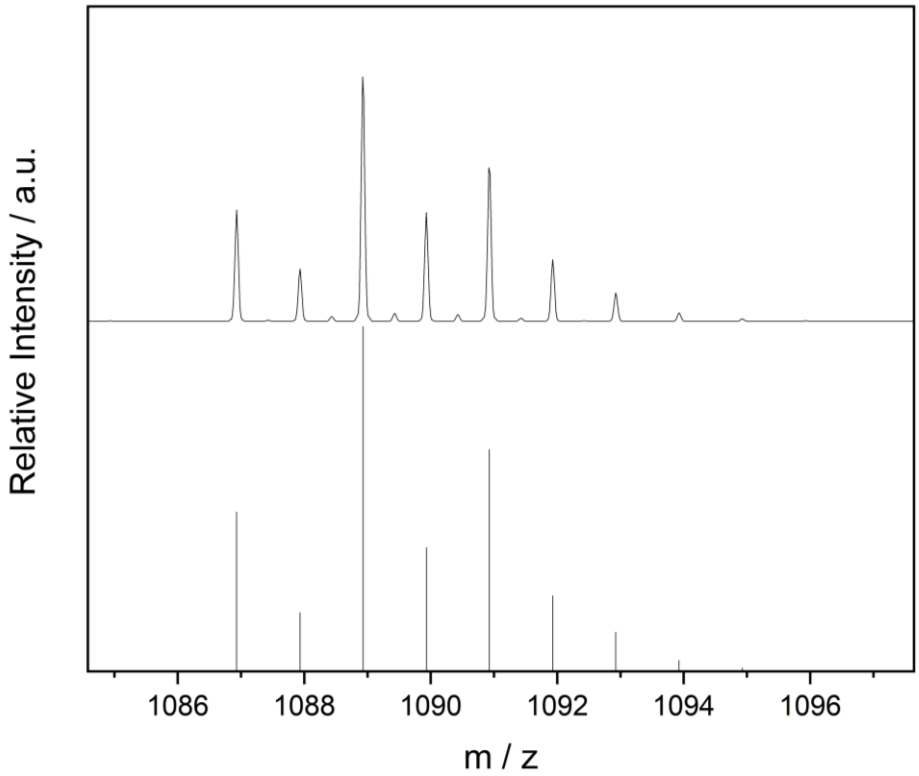

Figure S21: Measured molecule ion signals (m/z) of the HRESI-MS (top) and the theoretical isotopic pattern corresponding to $[H_6L^{Br2}(OTf)_3]^+$ (bottom).

8.2 HRESI-MS spectrum of $H_6L^{Br2}(PF_6)_4$

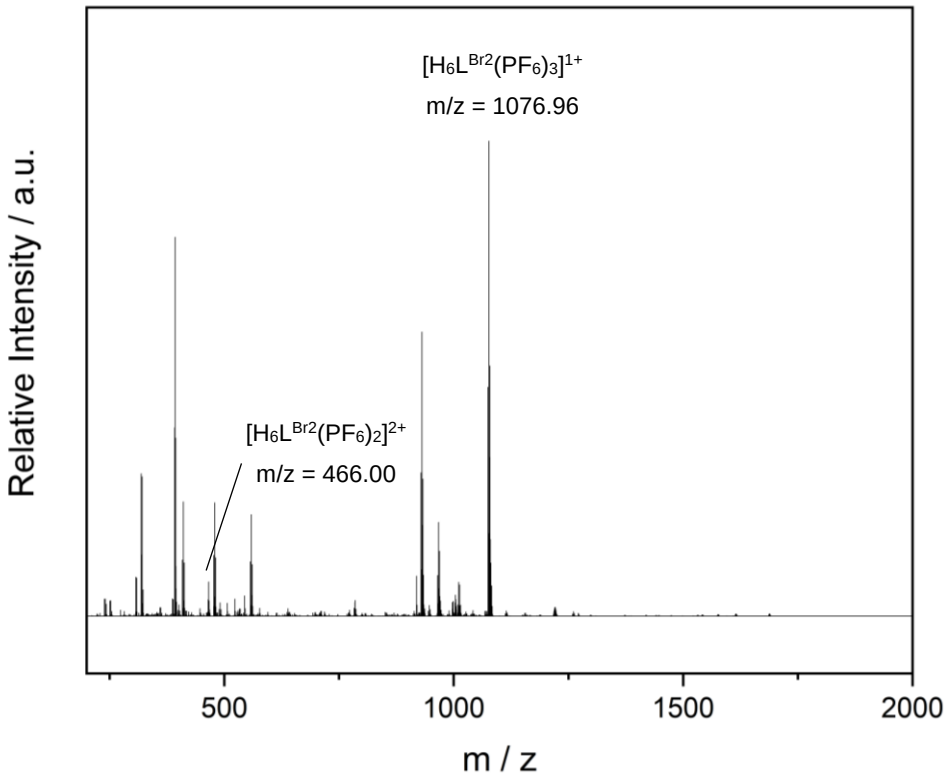

Figure S22: HRESI-MS spectrum of $H_6L^{Br2}(PF_6)_4$ in MeCN.

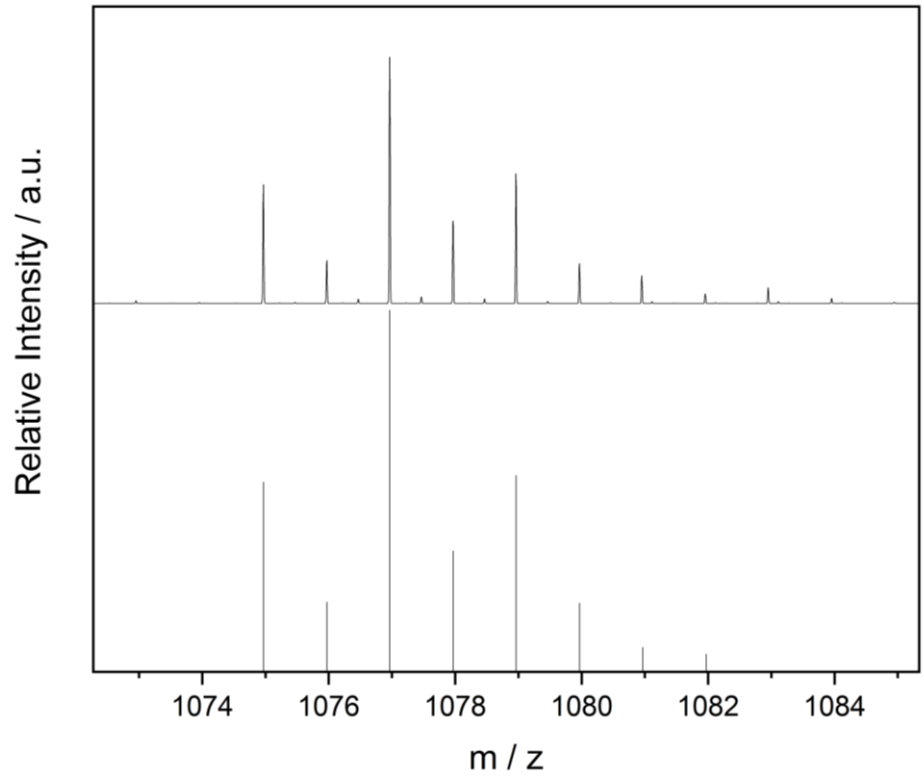

Figure S23: Measured molecule ion signals (m/z) of the HRESI-MS (top) and the theoretical isotopic pattern corresponding to $[H_6L^{Br2}(PF_6)_3]^+$ (bottom).

8.3 HRESI-MS spectrum of $Ag_8(L^{Br2})_2(PF_6)_4$

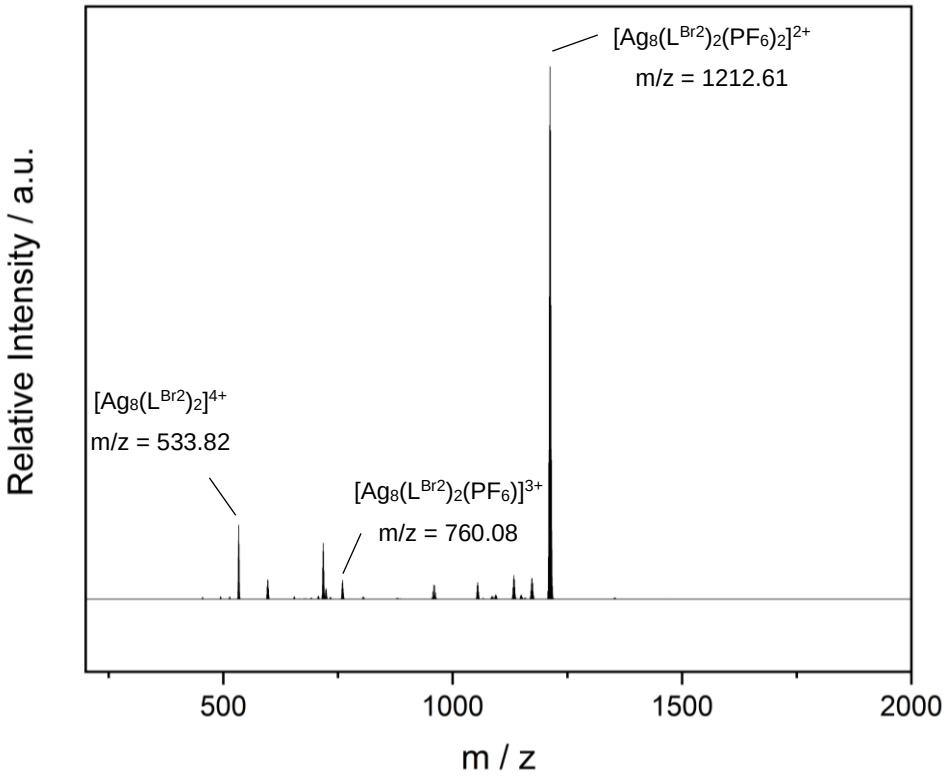

Figure S24: HRESI-MS spectrum of $Ag_8(L^{Br2})_2(PF_6)_4$ in MeCN.

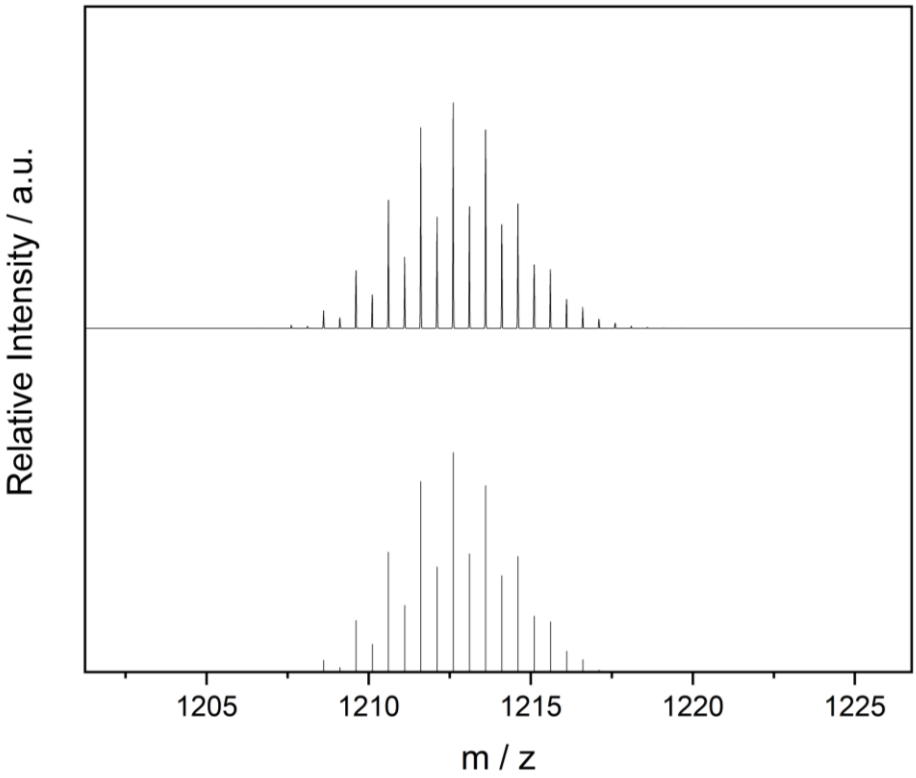

Figure S25: Measured molecule ion signals (m/z) of the HRESI-MS (top) and the theoretical isotopic pattern corresponding to $[Ag_8(L^{Br2})_2(PF_6)_3]^{2+}$ (bottom).

8.4 HRESI-MS spectrum of $Au_8(L^{Br2})_2(PF_6)_4$

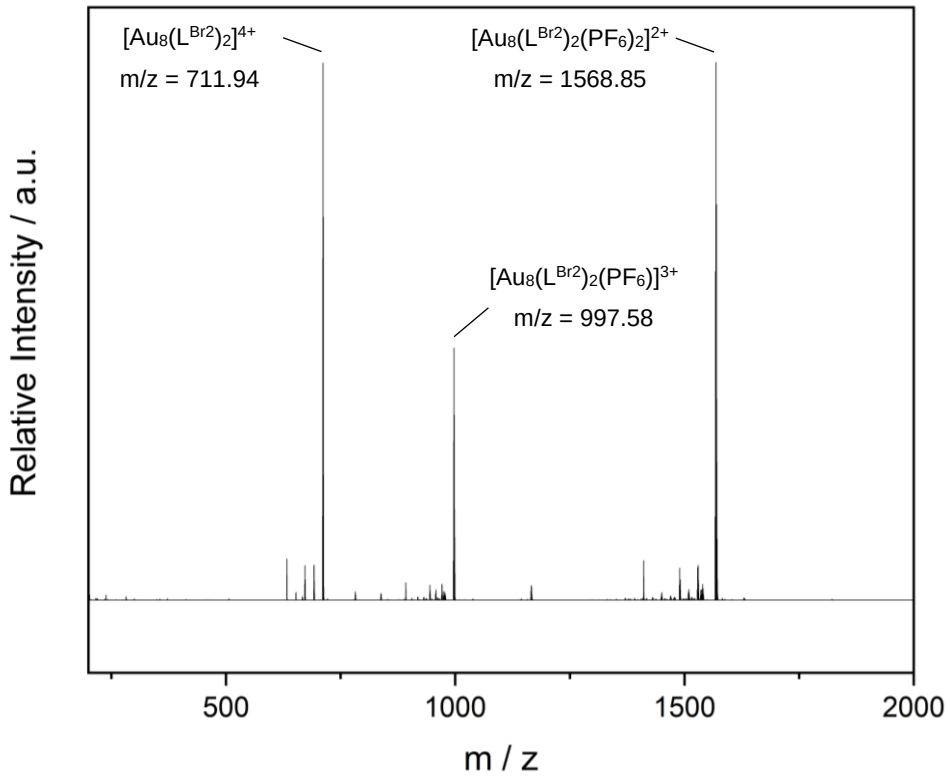

Figure S26: HRESI-MS spectrum of $Au_8(L^{Br2})_2(PF_6)_4$in MeCN.

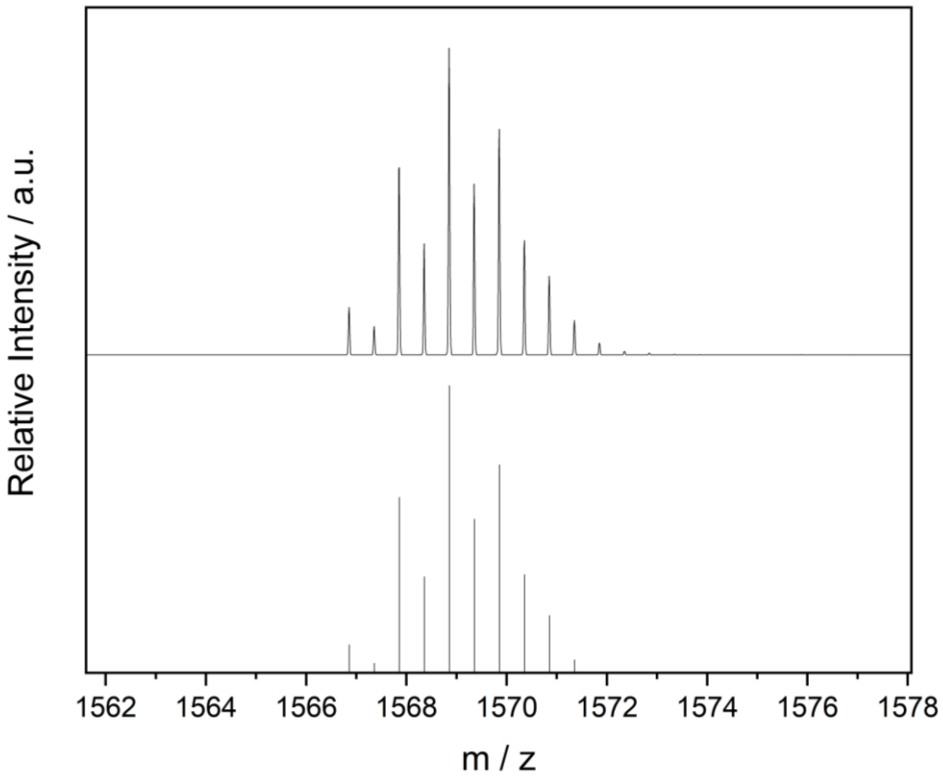

Figure S27: Measured molecule ion signals (m/z) of the HRESI-MS (top) and the theoretical isotopic pattern corresponding to $[Au_8(L^{Br2})_2(PF_6)_3]^{2+}$ (bottom).

9. Self-Sorting Experiments

9.1 HRESI-MS Studies

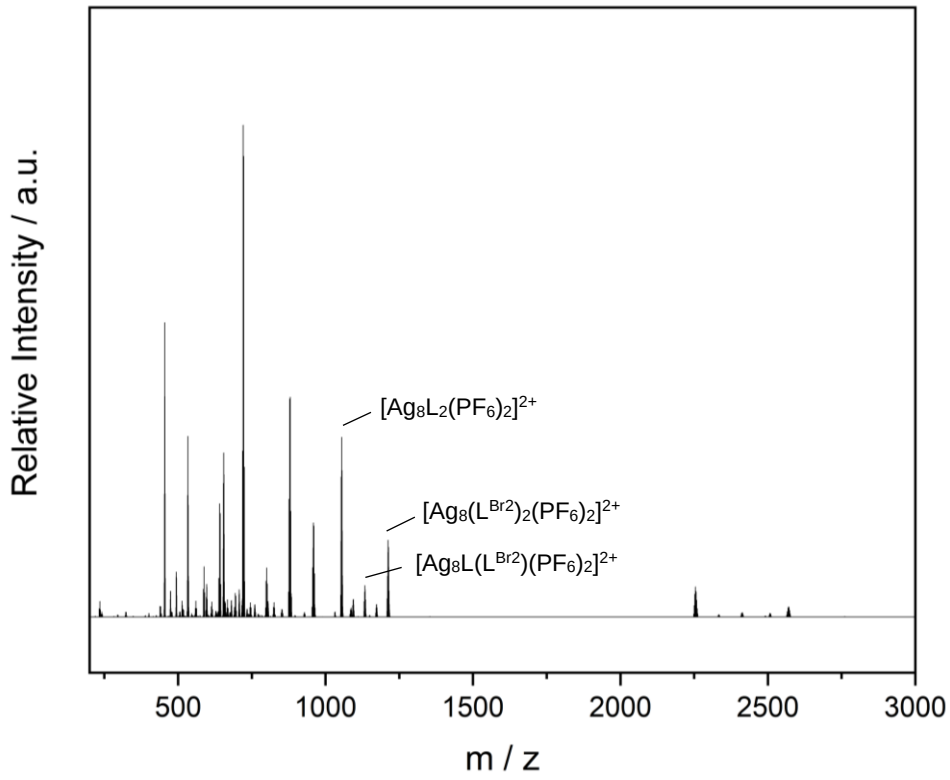

Figure S28: HRESI-MS spectrum of the reaction of $H_6L^{Br2}(PF_6)_4$, $H_6L(PF_6)_4$ and **5** equivalents of Ag_2O at room temperature after 16 h in MeCN-d_3.

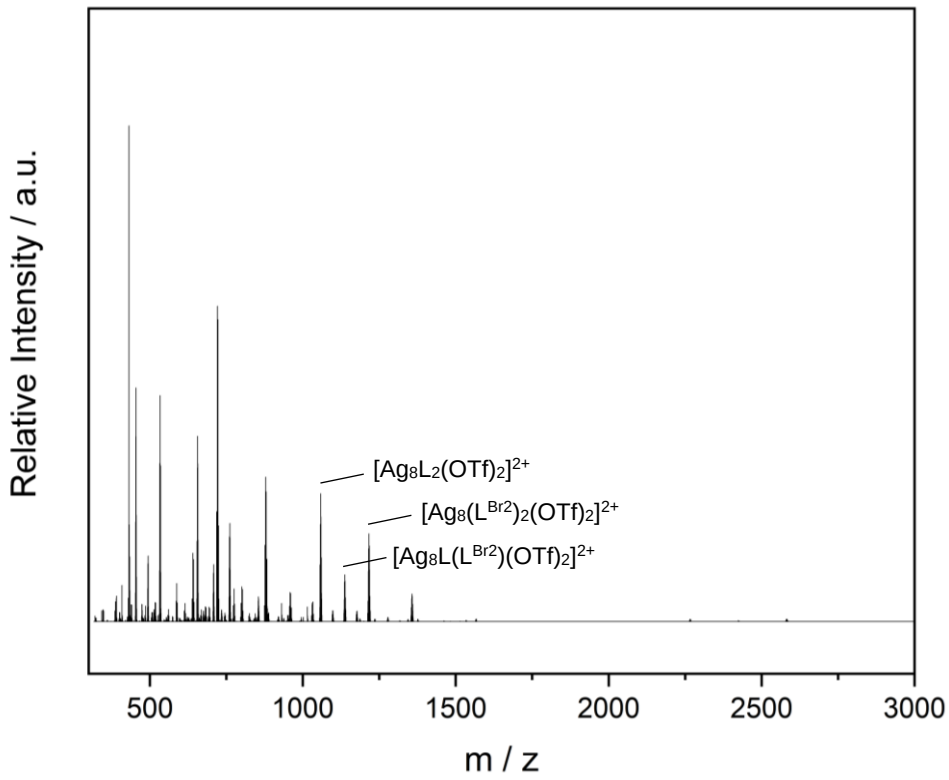

Figure S29: HRESI-MS spectrum of the reaction of $H_6L^{Br2}(OTf)_4$, $H_6L(OTf)_4$ and **5** equivalents of Ag_2O at room temperature after 16 h in MeCN-*d*$_3$.

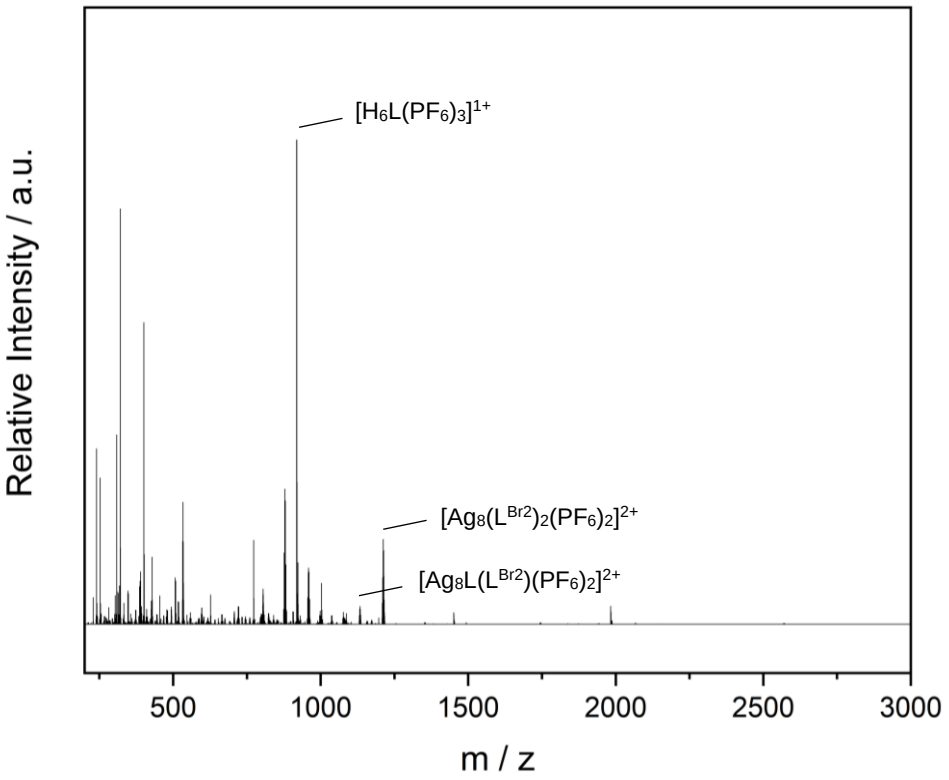

Figure S30: HRESI-MS spectrum of the reaction of $H_6L^{Br2}(PF_6)_4$, $H_6L(PF_6)_4$ and **2** equivalents of Ag_2O at room temperature after 16 h in MeCN-*d*$_3$.

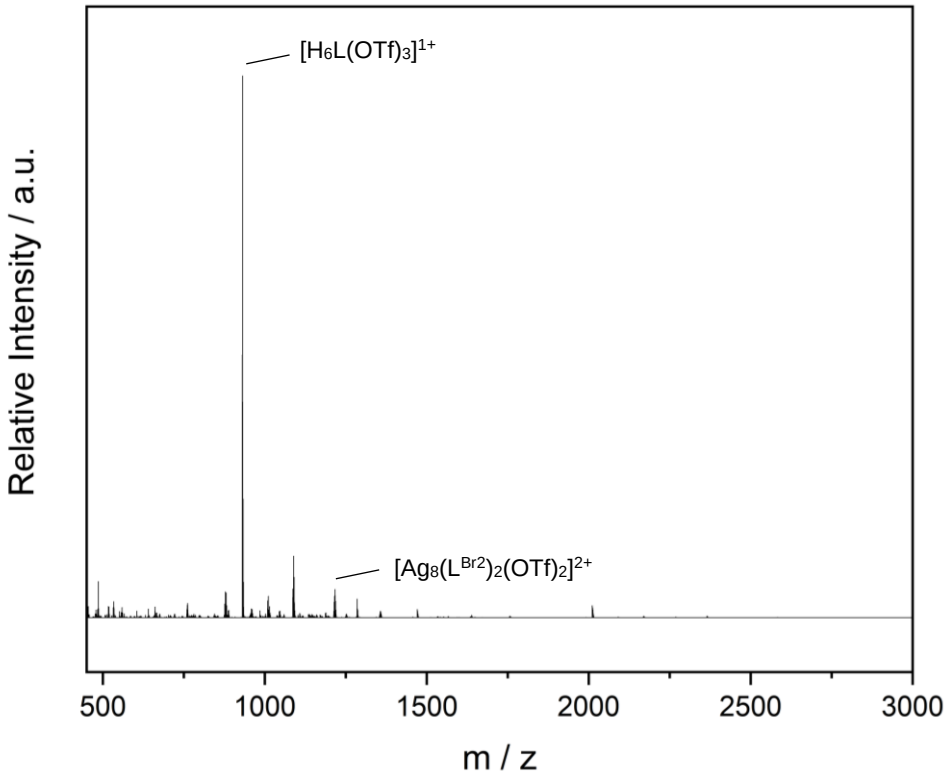

Figure S31: HRESI-MS spectrum of the reaction of $H_6L^{Br2}(OTf)_4$, $H_6L(OTf)_4$ and **2** equivalents of Ag_2O at room temperature after 16 h in MeCN-*d*$_3$.

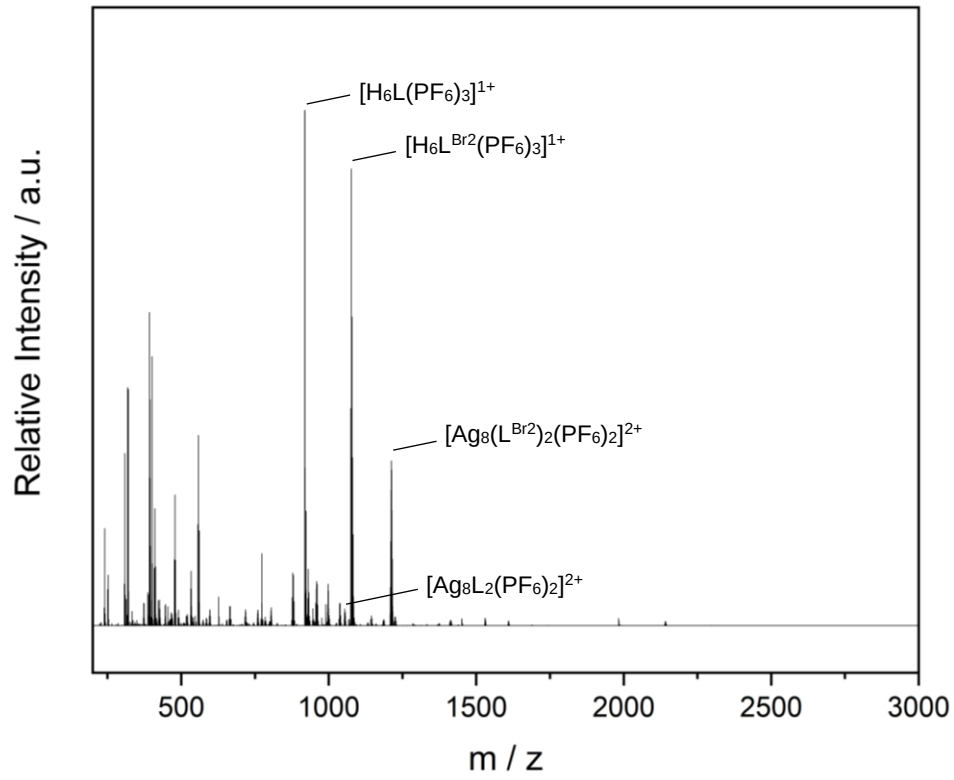

Figure S32: HRESI-MS spectrum of the ligand exchange reaction of $Ag_8L_2(PF_6)_4$ with **5** equivalents of $H_6L^{Br2}(PF_6)_4$ after 16 h at 50 °C in MeCN-*d*$_3$.

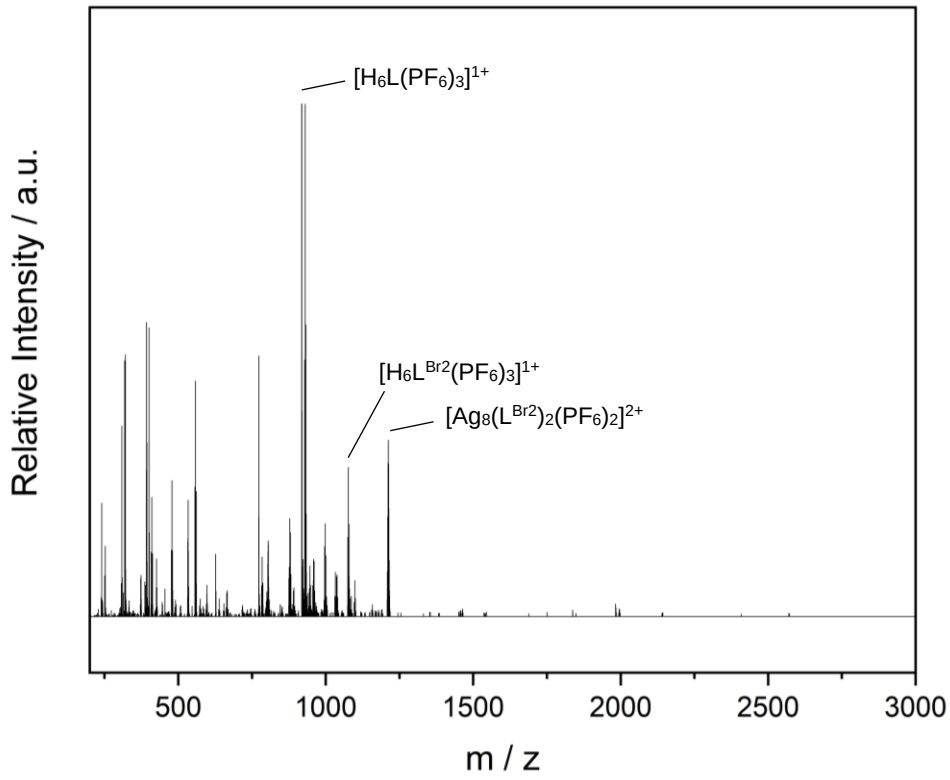

Figure 33: HRESI-MS spectrum of the ligand exchange reaction of $Ag_8L_2(PF_6)_4$ with **5** equivalents of $H_6L^{Br2}(PF_6)_4$ and **15** equivalents of NaOAc after 16 h at 50 °C in MeCN-d_3.

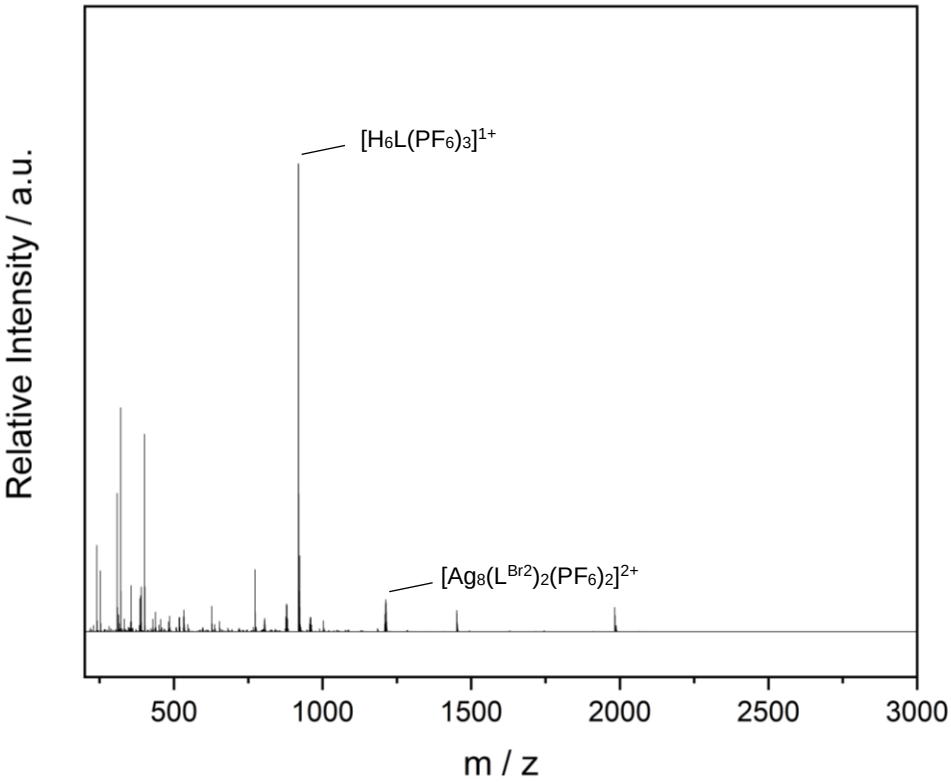

Figure S34: HRESI-MS spectrum of the control reaction experiment of $Ag_8(L^{Br2})_2(PF_6)_4$ with **5** equivalents of $H_6L(PF_6)_4$ after 16 h at 50 °C in MeCN-d_3.

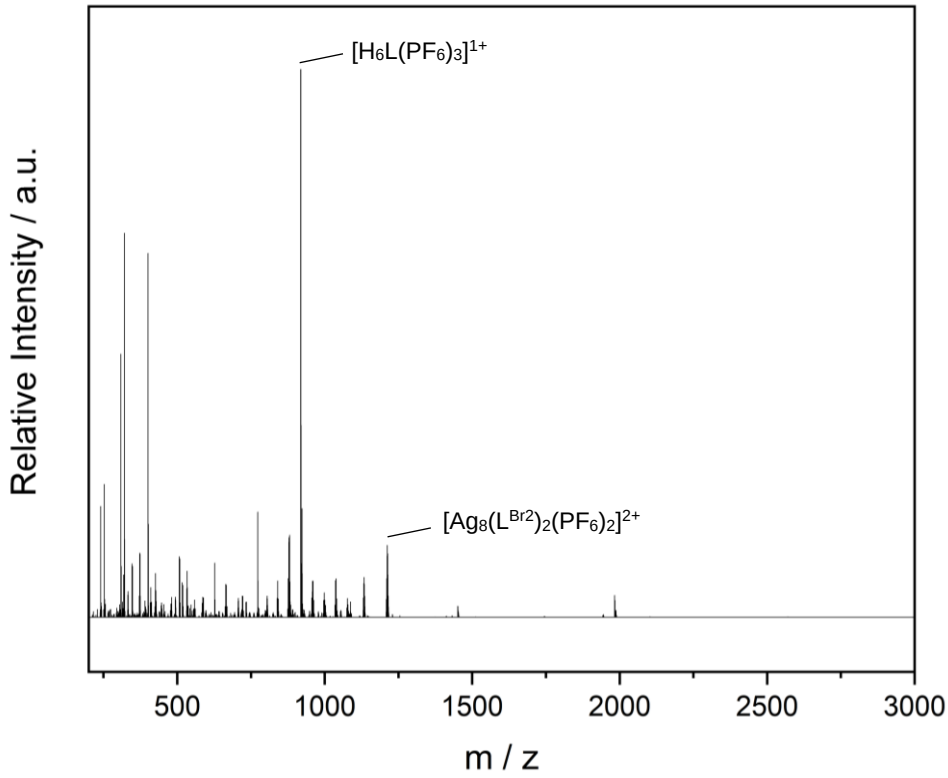

Figure S35: HRESI-MS spectrum of the control reaction experiment of $Ag_8(L^{Br2})_2(PF_6)_4$ with **5** equivalents of $H_6L(PF_6)_4$ and **15** equivalents of NaOAc after 16 h at 50 °C in MeCN-d_3.

9.2 NMR Studies

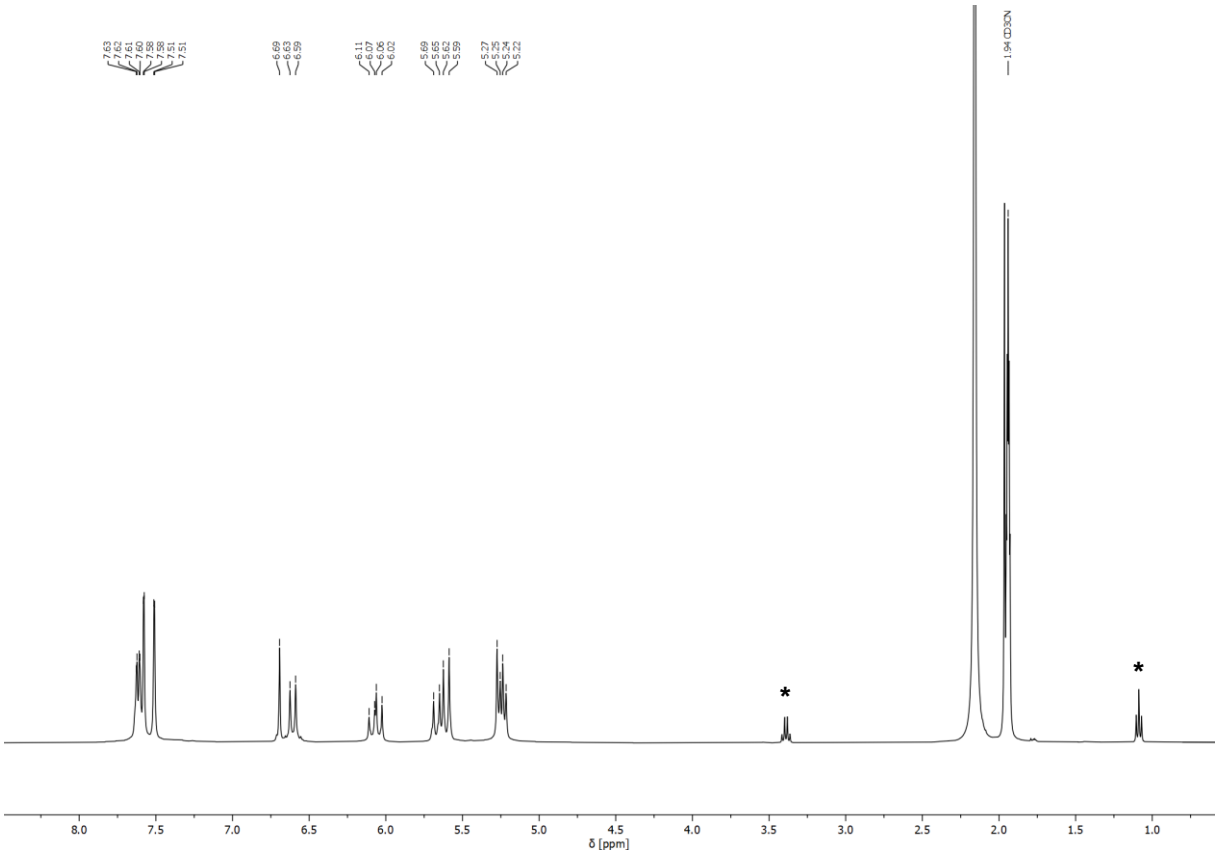

Figure S36: ^{1}H NMR spectrum of the reaction of $H_6L^{Br2}(PF_6)_4$, $H_6L(PF_6)_4$ and **5** equivalents of Ag_2O at room temperature after 16 h in MeCN-d_3 at 400 MHz. The signals marked by * are attributed to Et_2O.

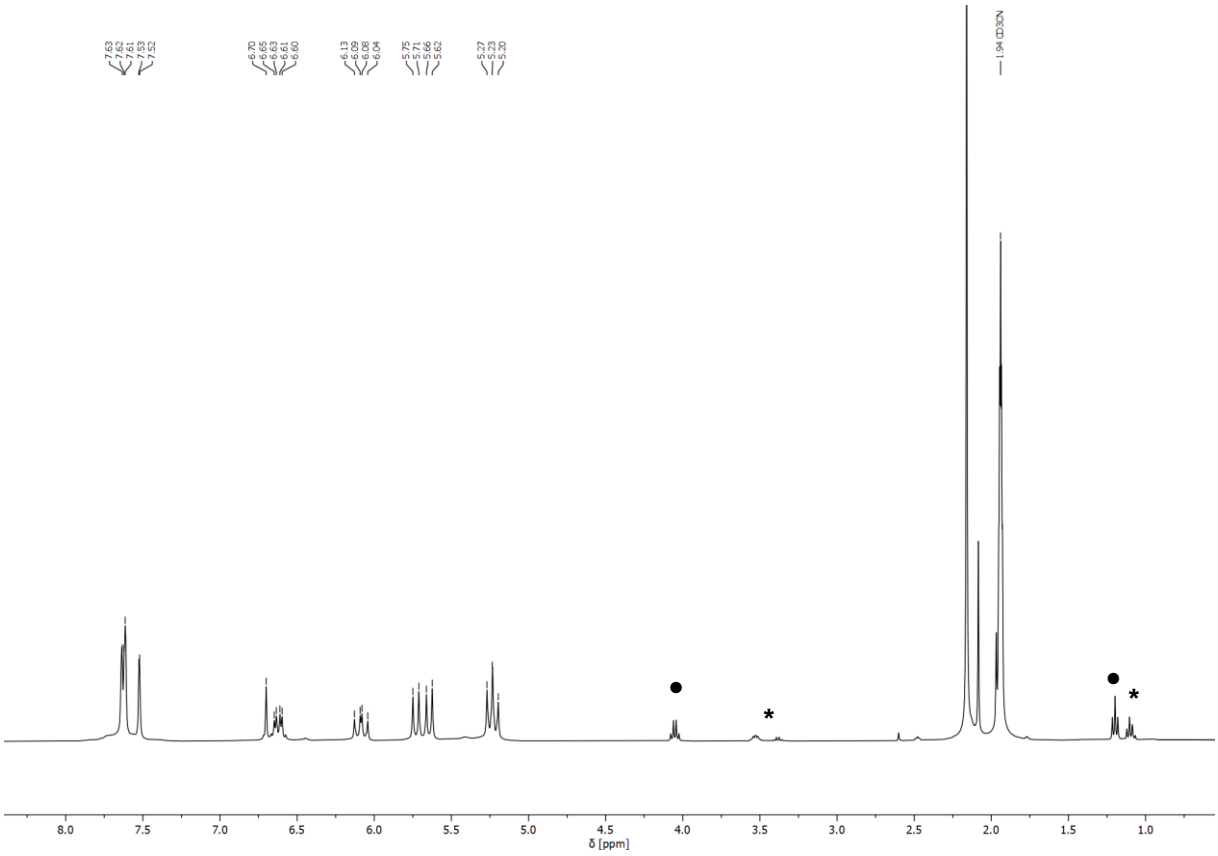

Figure S37: ^{1}H NMR spectrum of the reaction of $H_6L^{Br2}(OTf)_4$, $H_6L(OTf)_4$ and **5** equivalents of Ag_2O at room temperature after 16 h in MeCN-d_3 at 400 MHz. The signals marked by are attributed to Et_2O and ● belong to EtOAc.

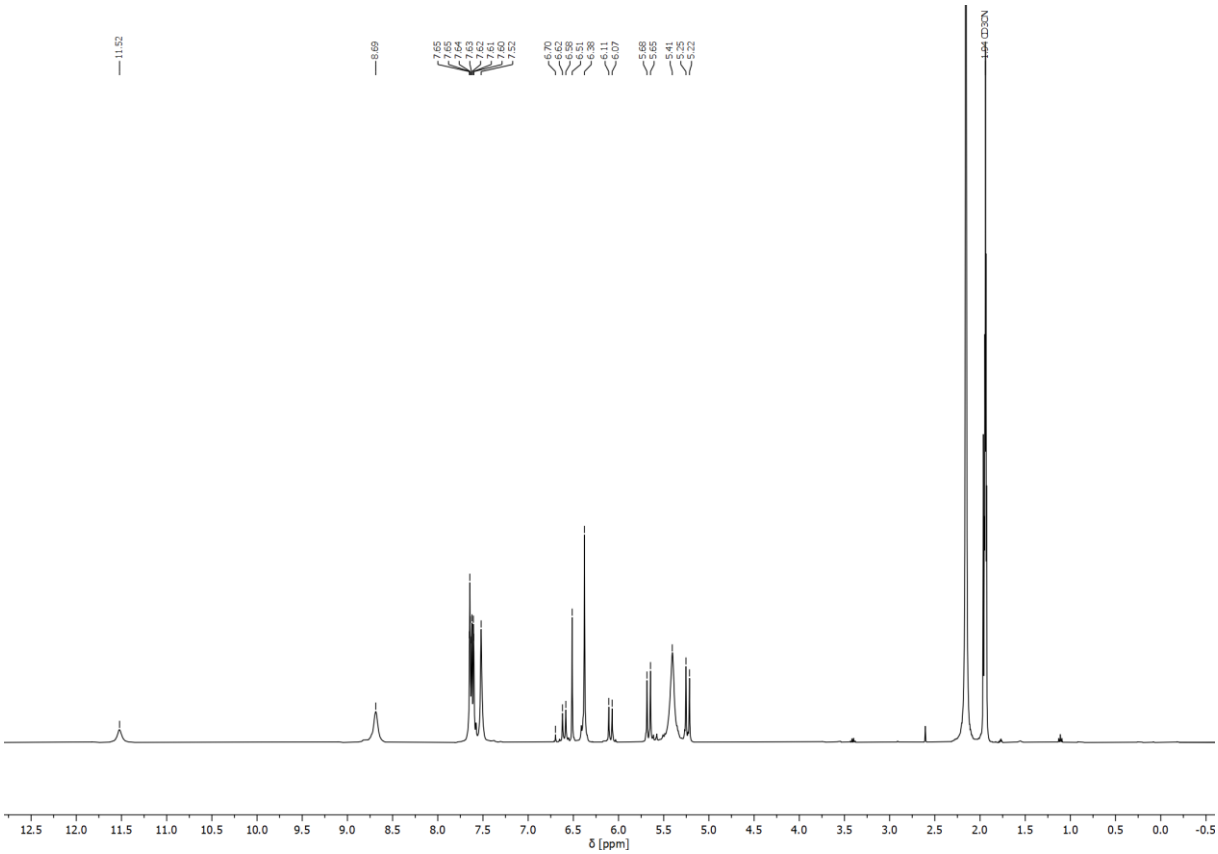

Figure S38: ^{1}H NMR spectrum of the reaction of $H_6L^{Br2}(PF_6)_4$, $H_6L(PF_6)_4$ and **2** equivalents of Ag_2O at room temperature after 16 h in MeCN-d_3 at 400 MHz.

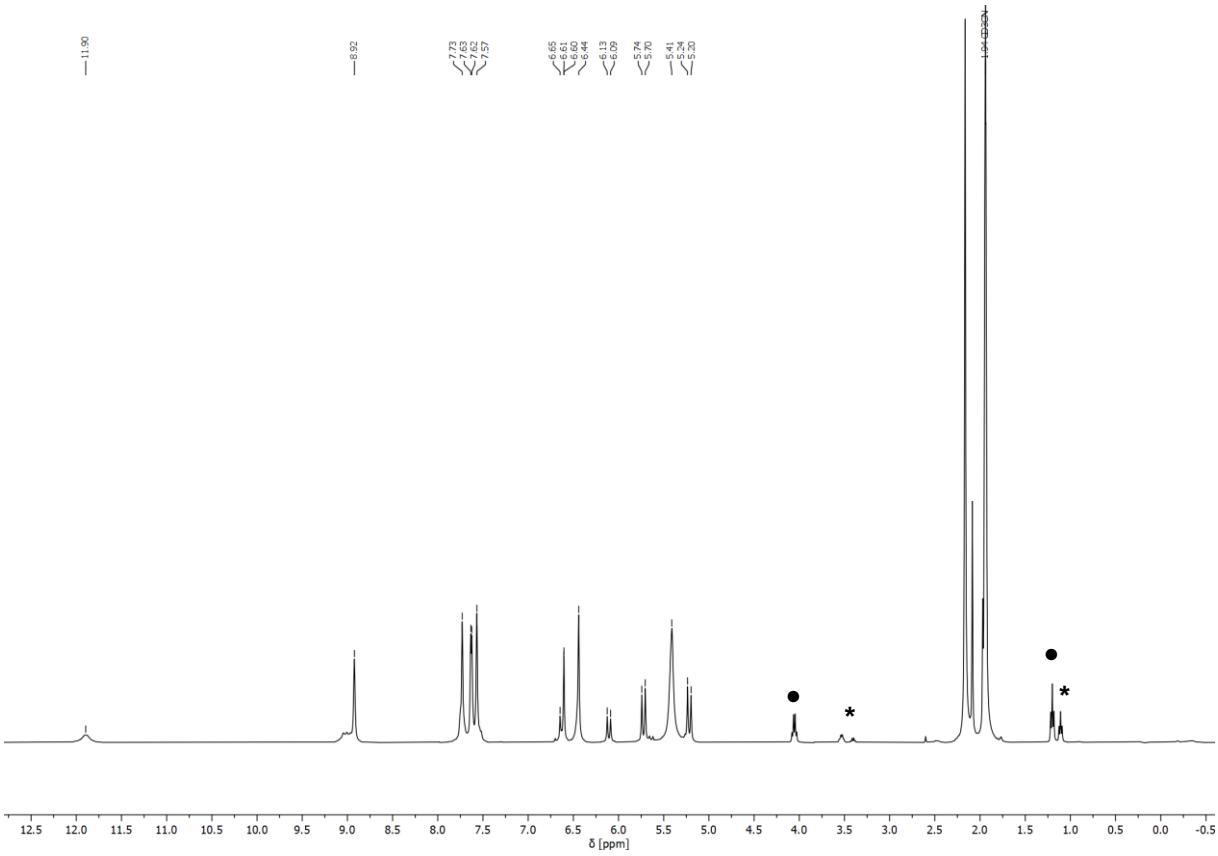

Figure S39: ^{1}H NMR spectrum of the reaction of $H_6L^{Br2}(OTf)_4$, $H_6L(OTf)_4$ and **2** equivalents of Ag_2O at room temperature after 16 h in MeCN-d_3 at 400 MHz. The signals marked by * are attributed to Et_2O and ● are attributed to EtOAc.

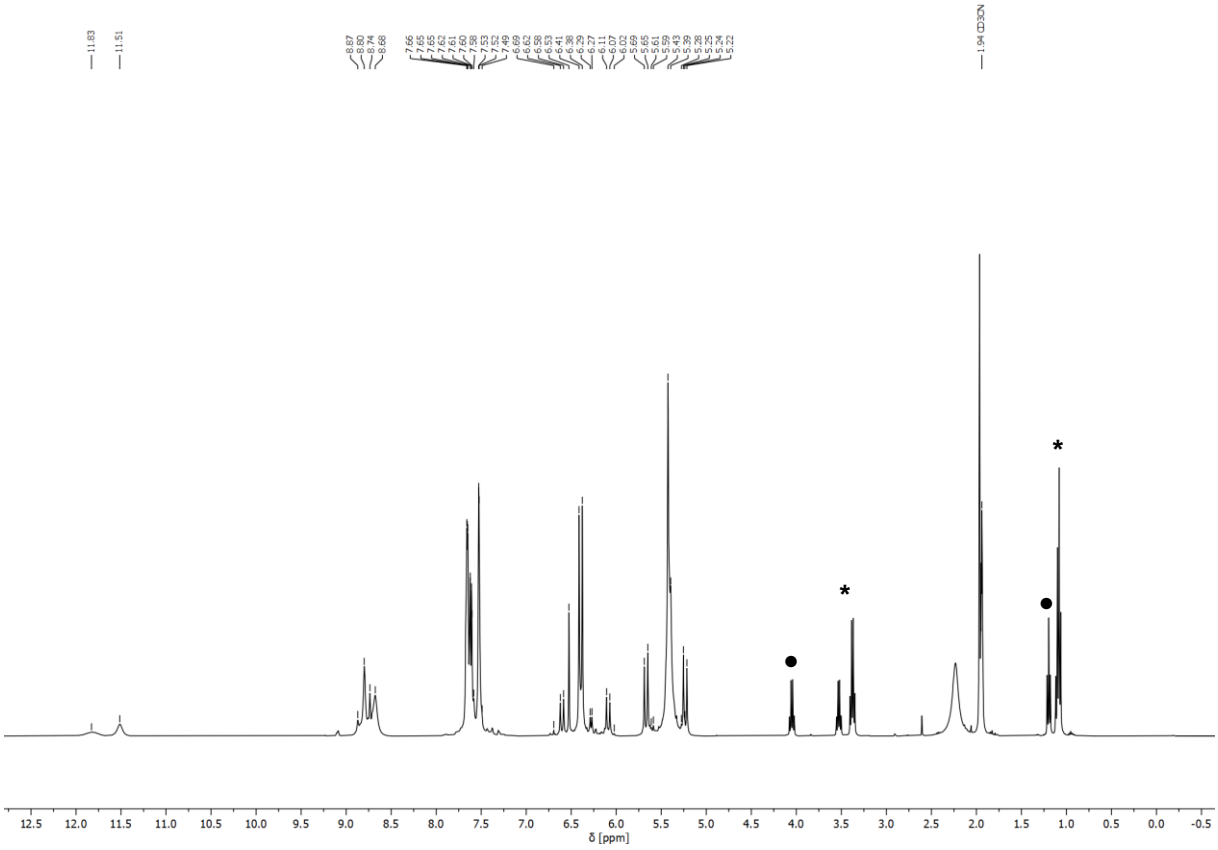

Figure S40: ^{1}H NMR spectrum of the ligand exchange reaction of $Ag_8L_2(PF_6)_4$ with **5** equivalents of $H_6L^{Br2}(PF_6)_4$ after 16 h at 50 °C in MeCN-d_3 at 400 MHz. The signals marked by * are attributed to Et_2O and ● are attributed to EtOAc.

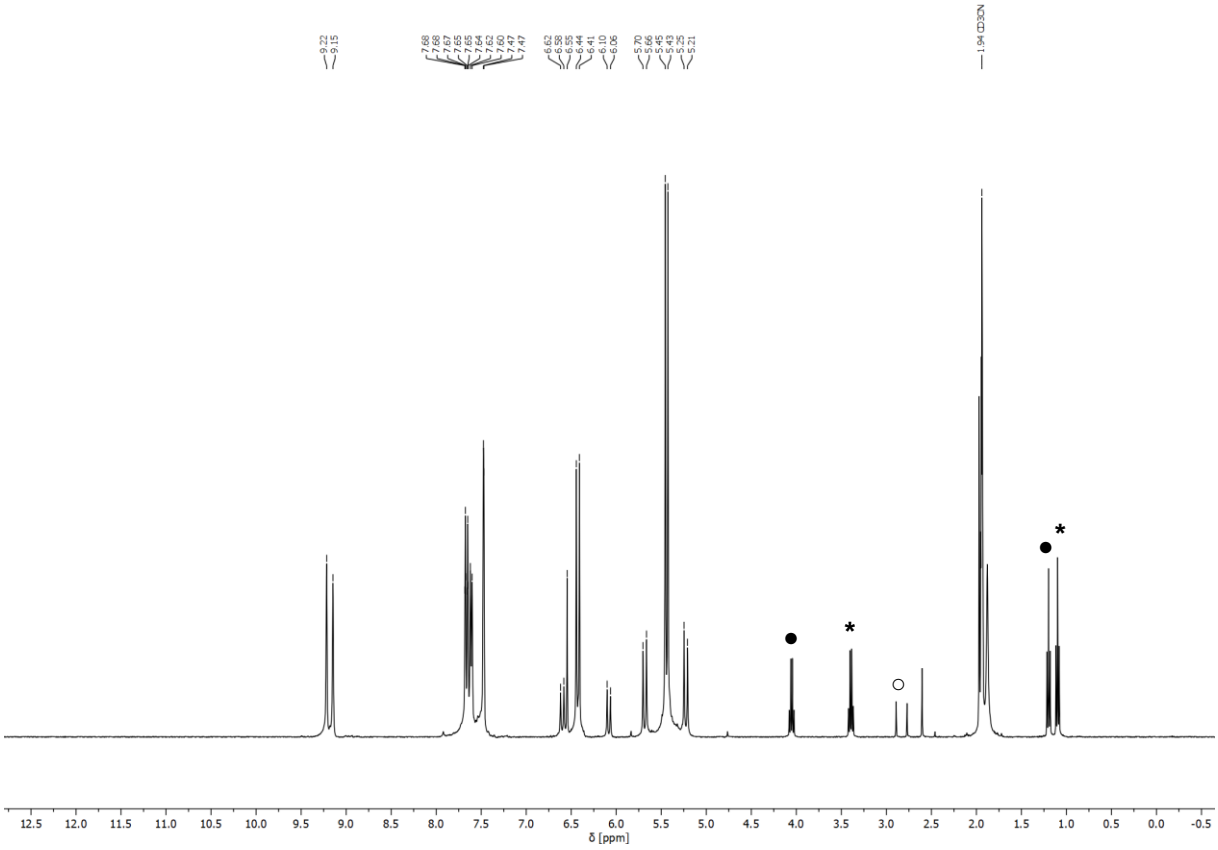

Figure S41: ^{1}H NMR spectrum of the ligand exchange reaction of $Ag_8L_2(PF_6)_4$ with **5** equivalents of $H_6L^{Br2}(PF_6)_4$ and **15** equivalents of NaOAc after 16 h at 50 °C in MeCN-d_3 at 400 MHz. The signals marked by * are attributed to Et_2O, ● are attributed to EtOAc and ○ belong to NBS.

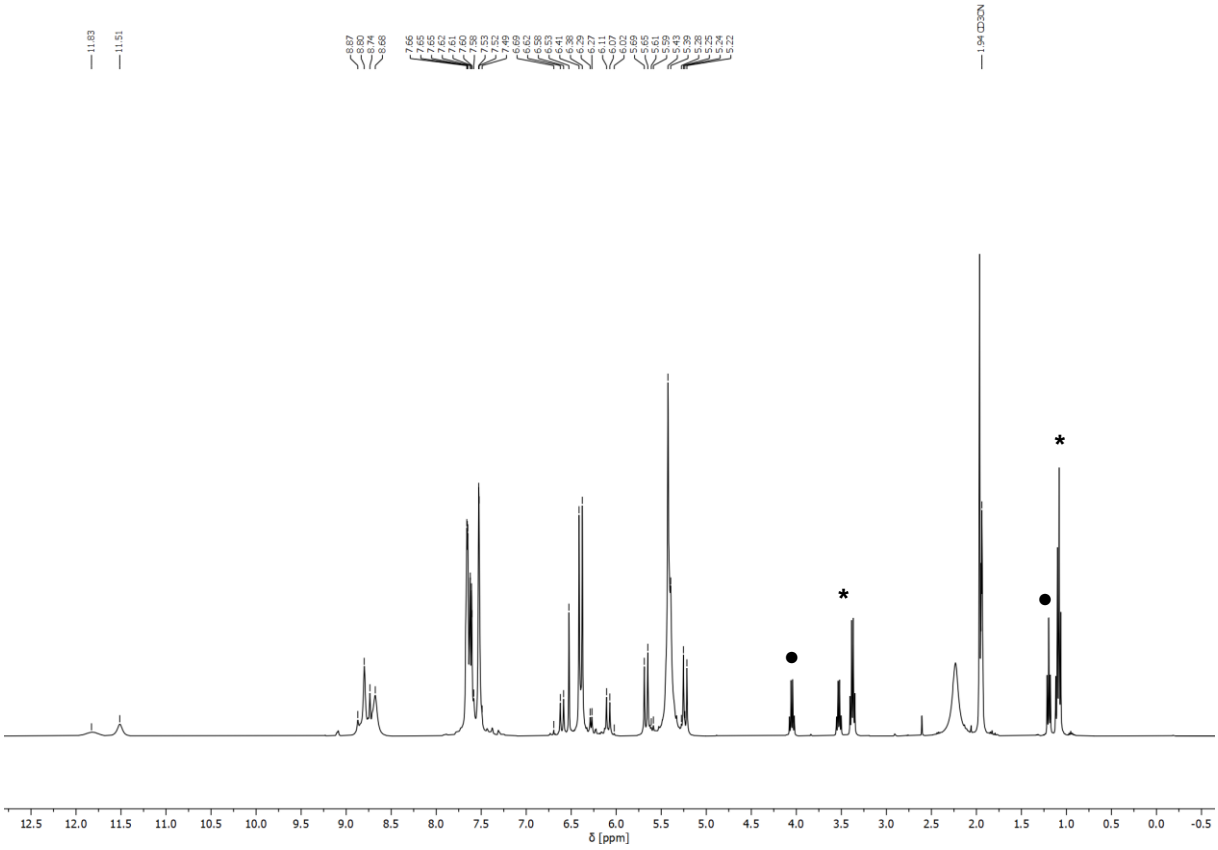

Figure S42: ^{1}H NMR spectrum of the control reaction experiment of $Ag_8(L^{Br2})_2(PF_6)_4$ with **5** equivalents of $H_6L(PF_6)_4$ after 16 h at 50 °C in MeCN-d_3 at 400 MHz. The signals marked by * are attributed to Et_2O and ● are attributed to EtOAc.

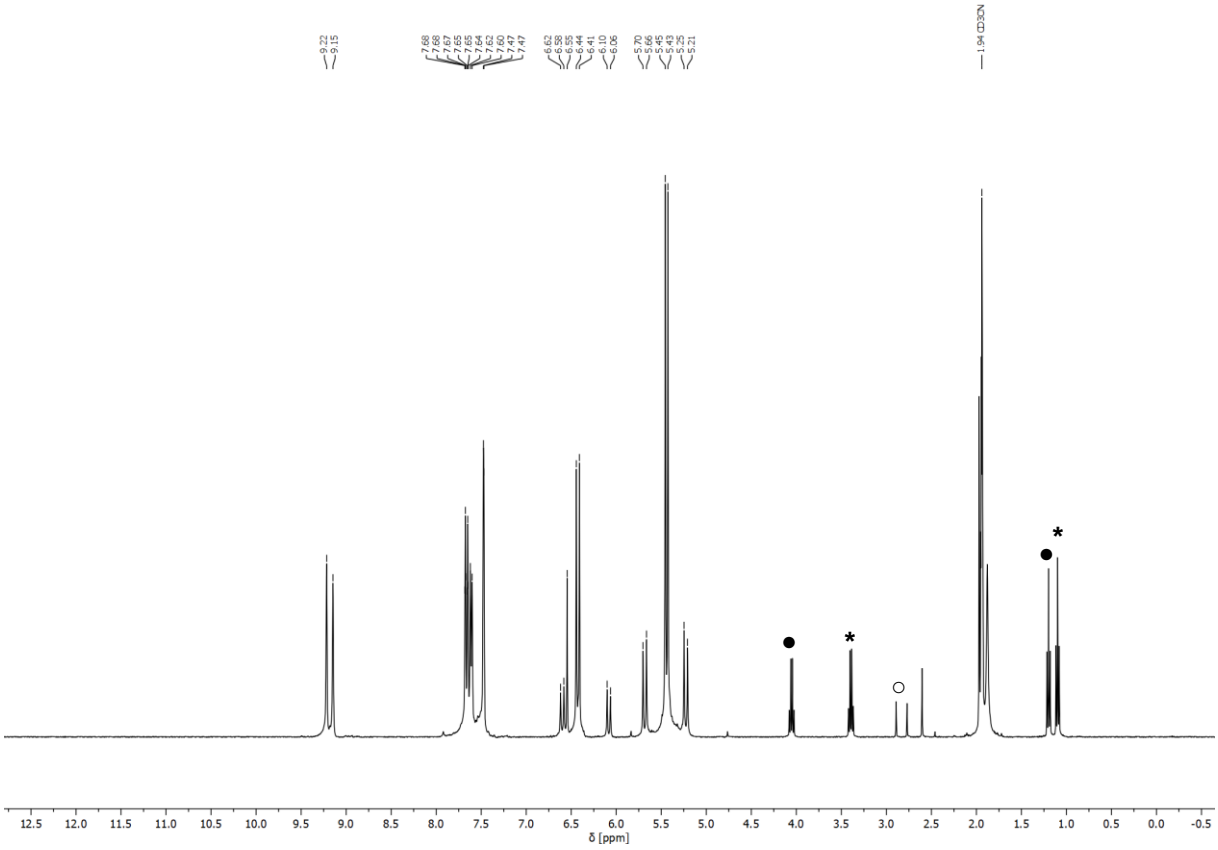

Figure S43: ^{1}H NMR spectrum of the control reaction experiment of $Ag_8(L^{Br2})_2(PF_6)_4$ with **5** equivalents of $H_6L(PF_6)_4$ and **15** equivalents of NaOAc after 16 h at 50 °C in MeCN-d_3 at 400 MHz. The signals marked by * are attributed to Et_2O, ● are attributed to EtOAc and ○ are attributed to NBS.

10. Computational Methods

Thermochemical DFT calculations were performed with the ORCA 5.0.4 quantum chemistry package[2, 3] on two different levels of theory:

1. The PBE0 exchange-correlation functional and the def2-TZVP triple-ξ valence basis set was used as implemented in ORCA.[4, 5] To account for relativistic effects, a full Stuttgart–Dresden effective core potential (def2-ECP) for Ag was employed for pillarplex cations.[6] To account for dispersion interactions, Grimme's atom-pairwise dispersion correction (D3) with the Becke-Johnson damping scheme (BJ) was applied.[7, 8]
2. The ωB97X-D4 range-separated hybrid functional including Grimme's atom-pairwise dispersion correction (D4) and the def2-TZVP triple-ξ valence basis set was used as implemented in ORCA.[5, 9, 10, 11] To account for relativistic effects, a full Stuttgart–Dresden effective core potential (def2-ECP) for Ag was employed for pillarplex cations.[6]

The conductor-like polarisable continuum model (CPCM) for acetonitrile was used to account for solvent effects. Tighter than normal SCF convergence criteria (TightSCF), finer than default grids (DefGrid3), tighter than normal convergence criteria for geometry optimisations (TightOPT), and the 'resolution-of-identity' (RI-J) approximation for Coulomb integrals as well as numerical chain-of-sphere integration for the HF Exchange

integrals (COSX) with the def2/J auxiliary basis set were employed as implemented in ORCA.[12] Starting geometries of the pillarplex cations ($[Ag_8L_2]^{4+}$, $[Ag_8L_2]^{4+}$) were obtained from the SC-XRD structure of $[Ag_8(L^{Br2})_2](PF_6)_4$. For proligands $[H_6L]^{4+}$ and $[H_6L^{Br2}]^{4+}$, the starting geometries are based on conformers which are structurally as close as possible to the ligand conformers in the pillarplexes (*i.e.* the geometry optimisations of the proligands were started in 'pillarplex' conformation). Geometries were optimised without symmetry constraints. Frequency analysis at the chosen level of theory confirmed that the optimisations had converged to an energetic minimum. Thermochemical data (at 298.15 K and 1.00 atm) were used as provided by ORCA. **NOTE:** Despite very rigorous grid settings (AngularGrid 7; IntAcc 7.0; AngularGridX 7,7,7,7,7; IntAccX 7.0; HessGridX = 7,7,7,7), SCF convergence criteria (VeryTightSCF), and convergence criteria for geometry optimisations (VeryTightOPT), a single negative eigenfrequency (–26 cm^{-1}) of the optimised structure of $[H_6L^{Br2}]^{4+}$ could not be removed. However, the thermochemical parameters of the ligand exchange reaction are not expected to be drastically affected by this.

Thermochemical DFT calculations – Detailed Results

The exchange reaction of pristine pillarplex $[Ag_8L_2]^{4+}$ with brominated ligand $[H_6L^{Br2}]^{4+}$ to afford brominated pillarplex $[Ag_8(L^{Br2})_2]^{4+}$ and pristine ligand $[H_6L]^{4+}$ in MeCN were calculated by DFT. Derived from the frequency analysis of the optimised structures on the PBE0-D3/def2-TZVP/CPCM level of theory, the Gibbs free energy for the reaction was calculated to be negative (ΔG_R = –25.2 kJ mol^{-1}), with a significant enthalpic contribution (ΔH_R = –25.0 kJ mol^{-1}, $T\Delta S_R$ = –0.2 kJ mol^{-1}). Higher-level geometry optimisations and frequency analyses at the ωB97X-D4/def2-TZVP/CPCM level of theory support the exergonicity of the reaction (ΔG_R = –43.6 kJ mol^{-1}), albeit suggesting additional beneficial entropic influence (ΔH_R = –31.2 kJ mol^{-1}, $T\Delta S_R$ = –12.4 kJ mol^{-1}).

DFT calculations involving constrained bond distances (i.e. calculations where the pore opening of $[Au_8(L^{Br2})_2]^{4+}$ was varied) were performed with the ORCA 5.0.4 quantum chemistry package.[2, 3] The PBE exchange-correlation functional and the def2-TZVP triple-ξ valence basis set was used as implemented in ORCA.[4, 5] To account for relativistic effects, a full Stuttgart–Dresden effective core potential (def2-ECP) for Au was employed for pillarplex cations.[6] To account for dispersion interactions, Grimme's atom-pairwise dispersion correction (D3) with the Becke-Johnson damping scheme (BJ) was applied.[7, 8] Tighter than normal SCF convergence criteria (TightSCF), default grids (DefGrid2), normal convergence criteria for geometry optimisations (OPT), and the 'resolution-of-identity' (RI-J) approximation for Coulomb integrals as well as numerical chain-of-sphere integration for the HF Exchange integrals (COSX) with the def2/J auxiliary basis set were employed as implemented in ORCA.[12] The starting geometry of $[Au_8(L^{Br2})_2]^{4+}$ was obtained from the SC-XRD structure of $[Au_8(L^{Br2})_2](PF_6)_4$. Geometries were optimised without symmetry constraints but with bond constrains, if applicable. Frequency analysis of freely optimised $[Au_8(L^{Br2})_2]^{4+}$ at the chosen level of theory confirmed that the unconstrained optimisation had converged to an energetic minimum.

The influence of the portal opening of both complexes on their total energy was assessed by incrementally constraining the distance defined by the outermost NHC backbone carbon atoms (NHC-pyrazole-NHC, NHC-bromopyrazole-NHC-triazole-NHC) – for further information see ref. **13** and Figure S44. The total energy E_{SP} obtained by a single point calculation of the (fully and partially) optimised structures of $[Au_8(L^{Br2})_2]^{4+}$ was found

to depend on the portal opening d_{calcd}, defined as the distance between the respective hydrogen atoms attached to the constrained NHC backbone carbons after subtraction of 2 × the covalence radius r_{cov} of hydrogen (2 x 0.32 A).[13, 14] A second-degree polynomial regression was used to accurately correlate the relative total energy ΔE_{SP} (kJ mol^{-1}) of **[Au$_8$L$_2$]$^{4+}$**, **[Au$_8$(L^{Br2})$_2$]$^{4+}$** and **[Au$_8$L$^t_2$]$^{4+}$** with the portal opening d_{calcd} (Å) of the complexes. The following functions were used to calculate the energies associated with selected portal openings:

[Au$_8$L$^t_2$]$^{4+}$: $\Delta E(d_{calcd}) = 19.03 \cdot (d_{calcd})^2 - 177.01 \cdot (d_{calcd}) + 411.92$
[Au$_8$L$_2$]$^{4+}$: $\Delta E(d_{calcd}) = 20.77 \cdot (d_{calcd})^2 - 229.11 \cdot (d_{calcd}) + 632.39$
[Au$_8$(L^{Br2})$_2$]$^{4+}$: $\Delta E(d_{calcd}) = 20.69 \cdot (d_{calcd})^2 - 237.47 \cdot (d_{calcd}) + 680.34$

The regression data and fittings for **[Au$_8$L$_2$]$^{4+}$** and **[Au$_8$L$^t_2$]$^{4+}$** were updated from ref. **13**.

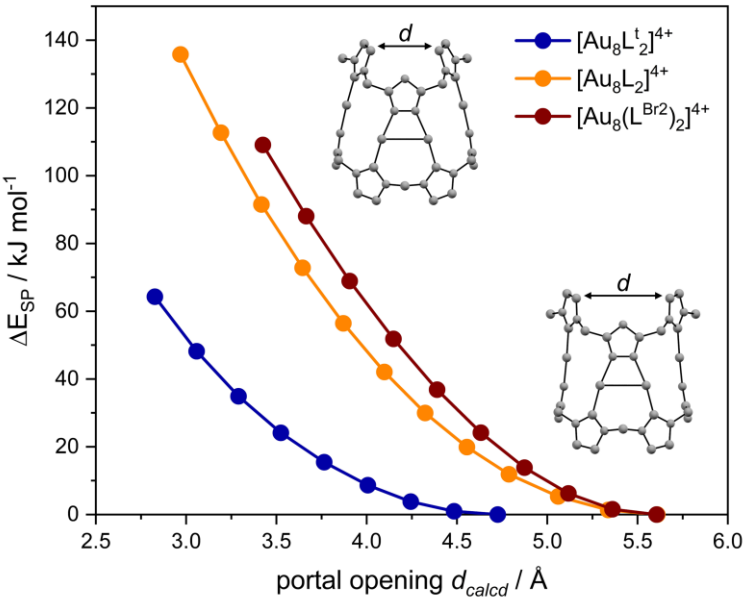

Figure S44: Calculated relative energy difference ΔE_{SP} of **[Au$_8$L$^t_2$]$^{4+}$**, **[Au$_8$L$_2$]$^{4+}$** and **[Au$_8$(L^{Br2})$_2$]$^{4+}$** as a function of the portal opening d_{calcd}. The relative energies of the unrestrained geometries of **[Au$_8$L$^t_2$]$^{4+}$**, **[Au$_8$L$_2$]$^{4+}$** and **[Au$_8$(L^{Br2})$_2$]$^{4+}$** serve as reference points and were set to zero.

11. Electron Diffraction

After gentle grinding between glass slides the sample of **$H_6L^{Br2}(OTf)_4$** was finely dispersed on a standard TEM grid (amorphous carbon on Cu) and measured on an ELDICO *ED-1* electron diffractometer at room temperature using the software ELDIX.[15] The device is equipped with a LaB_6 source operating at an acceleration voltage of 160 kV (λ = 0.02851 Å) and a hybrid-pixel detector (Dectris QUADRO). Suitable crystals were identified in STEM (scanning transmission electron microscopy) imaging mode and diffraction was recorded in continuous rotation mode with a beam diameter of ca. 750 nm. Parts of measurements showing significant beam damage or shadowing by the grid were omitted. Further data collection details are given in **Table S2**.

Table S2: ED data collection details for the crystals of $H_6L^{Br2}(OTf)_4$.

Crystal no.	Angular range [°]	Rotation per frame [°]	Exposure time [s]	Total exposure [s]	Frames measured	Frames used
1	−65 to +65	1	1	130	130	11 to 60
2	−10 to +65	1	1	75	75	1 to 30

11.1 Compound $H_6L^{Br2}(OTf)_4$ (2374511)

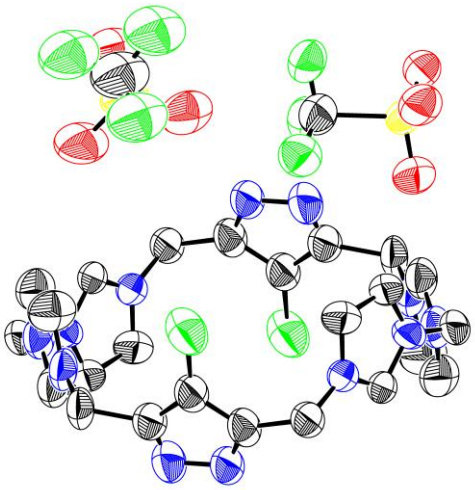

Figure S45: ORTEP representation of the solid-state structure of **$H_6L^{Br2}(OTf)_4$** (C = black, N = blue, O = red, F = light green, Br = green and S = yellow) shown with 50 % probability displacement ellipsoids. Two counterions are omitted for clarity.

Data were processed and evaluated using the APEX4 software package.[16] After unit cell determination the frames were integrated separately for each crystal, then merged, scaled, and corrected for Lorentz effects, scan speed, background, and absorption using SAINT and SADABS.[17, 18, 19] Space group determination was based on systematic absences, E statistics, and successful refinement of the structure. The structure was solved using ShelXD and refined with ShelXL in conjunction with ShelXle.[20, 21, 22] Least squares refinements were carried out within the kinematic approximation by minimising $\Sigma w(F_{obs}^2-F_{calc}^2)^2$ with the ShelXL weighting scheme and using neutral electron scattering factors.[22, 23] H atoms were placed in calculated positions based

on typical distances for neutron diffraction and refined with a riding model and $U_{iso}(H) = 1.2 \cdot U_{eq}(C)$. Restraints on geometries and anisotropic displacement parameters (ShelXL keywords SADI, SAME, SIMU, RIGU) were used to ensure convergence within physically reasonable limits. Deposition Number 2374511 contains the supplementary crystallographic data for this paper. These data are provided free of charge by the joint Cambridge Crystallographic Data Centre and Fachinformationszentrum Karlsruhe Access Structures service and can be accessed at www.ccdc.cam.ac.uk/structures.[24] Images of the solid-state structure were generated with *MERCURY*, *PLATON* and *PyMOL*.[25, 26, 27, 28]

Table S3: Crystal data and structure refinement for compound $H_6L^{Br2}(OTf)_4$.

CCDC number	2374511
Empirical formula	$C_{28}H_{26}Br_2F_{12}N_{12}O_{12}S_4$
Formula weight	1238.65
Temperature [K]	293
Crystal system	Orthorhombic
Space group (number)	*Pbca* (61)
a [Å]	12.8(3)
b [Å]	19.7(4)
c [Å]	20.2(4)
α [°]	90
β [°]	90
γ [°]	90
Volume [Å^3]	5094
Z	4
ρ_{calc} [gcm^{-3}]	1.620
Crystal size	nanocrystals
Crystal colour	colourless
Radiation	electrons, λ = 0.02851 Å
θ range [°]	0.09−0.74
Index ranges	$-11 \le h \le 11$, $-17 \le k \le 17$, $-15 \le l \le 14$
Reflections collected	5874
Independent reflections	1578
Completeness	0.787
Data / Restraints / Parameters	1578 / 499 / 317
Goodness of fit	1.08
Final *R* indexes [$I \ge 2\sigma(I)$]	R_1 = 0.2586, wR_2 = 0.5711
Final *R* indexes [all data]	R_1 = 0.3074, wR_2 = 0.6211
Largest peak/hole [eÅ^{-3}]	0.34/−0.18

12. Crystallographic details

12.1 Compound $H_6L^{Br2}(PF_6)_4$ (2374510)

SC-XRD structure report for compound $H_6L^{Br2}(PF_6)_4$.

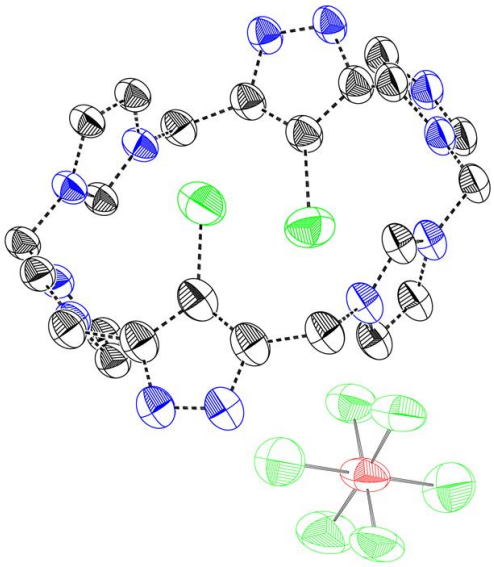

Figure S46: ORTEP representation of the solid-state structure of **$H_6L^{Br2}(PF_6)_4$** (C = black, N = blue, P = red, F = light green, Br = green and S = yellow) shown with 50 % probability displacement ellipsoids. Three counterions are omitted for clarity. Dashed lines indicate the whole molecule disorder of the cation.

A colourless, plate-shaped crystal of $C_{24}H_{26}Br_2F_{24}N_{12}P_4$ coated with perfluorinated ether and fixed on top of a Kapton micro sampler was used for X-ray crystallographic analysis. The X-ray intensity data were collected at 296(2) K on a Bruker D8 VENTURE Duo three-angle diffractometer with an IMS microsource with MoK_α radiation (λ=0.71073 Å) using APEX4.[16] The diffractometer was equipped with a Helios optic monochromator, a Bruker PHOTON II detector, and an Oxford Cryostreamlow temperature device.

A matrix scan was used to determine the initial lattice parameters. All data were integrated with the Bruker SAINT V8.40B software package using a narrow-frame algorithm and the reflections were corrected for Lorentz and polarisation effects, scan speed, and background.[17] The integration of the data using a monoclinic unit cell yielded a total of 31189 reflections within a 2θ range [°] of 3.97 to 41.63 (1.00 Å), of which 2533 were independent. Data were corrected for absorption effects including odd and even ordered spherical harmonics by the multi-scan method (SADABS 2016/2).[18, 19] Space group assignment was based upon systematic absences, E statistics, and successful refinement of the structure.

The structure was solved by direct methods using SHELXT and refined by full-matrix least-squares methods against F^2 by minimising $\Sigma w(F_o^2 - F_c^2)^2$ using SHELXL in conjunction with SHELXLE.[20, 21, 22] All non-hydrogen atoms were refined with anisotropic displacement parameters. Hydrogen atoms were refined isotropically on calculated positions using a riding model with their U_{iso} values constrained to 1.5 times the U_{eq} of their pivot atoms for terminal sp^3 carbon atoms and a C–H distance of 0.98 Å. Non-methyl hydrogen atoms were refined using a riding model with methylene, aromatic, and other C–H distances of 0.99 Å, 0.95 Å, and 1.00 Å, respectively, and U_{iso} values constrained to 1.2 times the U_{eq} of their pivot atoms.

Neutral atom scattering factors for all atoms and anomalous dispersion corrections for the non-hydrogen atoms were taken from International Tables for Crystallography.[29] Supplementary crystallographic data reported in this paper have been deposited with the Cambridge Crystallographic Data Centre (2374510) and can be obtained free of charge from The Cambridge Crystallographic Data Centre via www.ccdc.cam.ac.uk/structures.[24] This report and the CIF file were generated using FinalCif.[30] Images of the crystal structure were generated with *MERCURY*, *PLATON* and *PyMOL*.[25, 26, 27, 28]

Table S4: Crystal data and structure refinement for compound $H_6L^{Br2}(PF_6)_4$.

CCDC number	2374510
Empirical formula	$C_{24}H_{26}Br_2F_{24}N_{12}P_4$
Formula weight	1222.27
Temperature [K]	296(2)
Crystal system	monoclinic
Space group (number)	$C2/c$ (15)
a [Å]	10.703(6)
b [Å]	24.950(16)
c [Å]	18.538(10)
α [°]	90
β [°]	102.850(9)
γ [°]	90
Volume [Å^3]	4826(5)
Z	4
ρ_{calc} [gcm^{-3}]	1.682
μ [mm^{-1}]	1.940
F(000)	2400
Crystal size [mm^3]	0.116×0.163×0.395
Crystal colour	colourless
Crystal shape	plate
Radiation	MoK_α (λ=0.71073 Å)
2θ range [°]	3.97 to 41.63 (1.00 Å)
Index ranges	−10 ≤ h ≤ 10 −24 ≤ k ≤ 24 −18 ≤ l ≤ 18
Reflections collected	31189
Independent reflections	2533 R_{int} = 0.1037 R_{sigma} = 0.0508
Completeness to θ = 20.816°	100.0
Data / Restraints / Parameters	2533 / 4878 / 1072
Goodness-of-fit on F^2	1.073
Final *R* indexes [$I \geq 2\sigma(I)$]	R_1 = 0.0985 wR_2 = 0.2648
Final *R* indexes [all data]	R_1 = 0.1428 wR_2 = 0.3090
Largest peak/hole [eÅ^{-3}]	0.35/−0.28

12.2 Compound $Ag_8(L^{Br2})_2(PF_6)_4$ (2374512)

SC-XRD structure report for compound $Ag_8(L^{Br2})_2(PF_6)_4$.

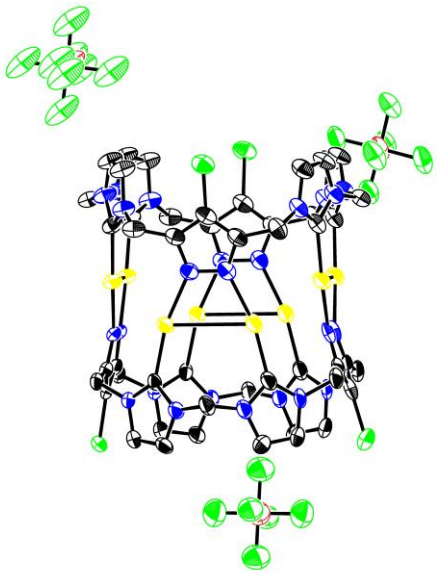

Figure S47: ORTEP representation of the solid-state structure of **$Ag_8(L^{Br2})_2(PF_6)_4$** (C = black, N = blue, P = red, F = light green, Br = green and Ag = yellow) shown with 50 % probability displacement ellipsoids. Solvent molecules and one counterion are omitted for clarity.

A colourless, plate-shaped crystal of $C_{48}H_{40}Ag_8Br_4F_{24}N_{24}P_4$ coated with perfluorinated ether and fixed on top of a Kapton micro sampler was used for X-ray crystallographic analysis. The X-ray intensity data were collected at 100(2) K on a Bruker D8 VENTURE Duo three-angle diffractometer with an IMS microsource with MoK_α radiation (λ=0.71073 Å) using APEX4.[16] The diffractometer was equipped with a Helios optic monochromator, a Bruker PHOTON II detector, and an Oxford Cryostreamlow temperature device.

A matrix scan was used to determine the initial lattice parameters. All data were integrated with the Bruker SAINT V8.40B software package using a narrow-frame algorithm and the reflections were corrected for Lorentz and polarisation effects, scan speed, and background.[17] The integration of the data using a orthorhombic unit cell yielded a total of 270041 reflections within a 2θ range [°] of 3.89 to 52.04 (0.81 Å), of which 12302 were independent. Data were corrected for absorption effects including odd and even ordered spherical harmonics by the multi-scan method (SADABS 2016/2).[18, 19] Space group assignment was based upon systematic absences, E statistics, and successful refinement of the structure.

The structure was solved by direct methods using SHELXT and refined by full-matrix least-squares methods against F^2 by minimising $\Sigma w(F_o^2 - F_c^2)^2$ using SHELXL in conjunction with SHELXLE.[20, 21, 22] All non-hydrogen atoms were refined with anisotropic displacement parameters. Hydrogen atoms were refined isotropically on calculated positions using a riding model with their U_{iso} values constrained to 1.5 times the U_{eq} of their pivot atoms for terminal sp^3 carbon atoms and a C–H distance of 0.98 Å. Non-methyl hydrogen atoms were refined using a riding model with methylene, aromatic, and other C–H distances of 0.99 Å, 0.95 Å, and 1.00 Å, respectively, and U_{iso} values constrained to 1.2 times the U_{eq} of their pivot atoms.

Neutral atom scattering factors for all atoms and anomalous dispersion corrections for the non-hydrogen atoms were taken from International Tables for Crystallography.[29] Supplementary crystallographic data

reported in this paper have been deposited with the Cambridge Crystallographic Data Centre (2374512) and can be obtained free of charge from The Cambridge Crystallographic Data Centre via www.ccdc.cam.ac.uk/structures.[24] This report and the CIF file were generated using FinalCif.[30] Images of the crystal structure were generated with *MERCURY*, *PLATON* and *PyMOL*.[25, 26, 27, 28]

Table S5: Crystal data and structure refinement for compound $Ag_8(L^{Br2})_2(PF_6)_4$.

CCDC number	2374512
Empirical formula	$C_{48}H_{40}Ag_8Br_4F_{24}N_{24}P_4$
Formula weight	2715.52
Temperature [K]	100(2)
Crystal system	orthorhombic
Space group (number)	$Pnma$ (62)
a [Å]	24.1945(15)
b [Å]	24.0406(15)
c [Å]	20.9494(13)
α [°]	90
β [°]	90
γ [°]	90
Volume [Å^3]	12185.2(13)
Z	4
ρ_{calc} [gcm^{-3}]	1.480
μ [mm^{-1}]	2.692
F(000)	5152
Crystal size [mm^3]	0.167×0.223×0.247
Crystal colour	colourless
Crystal shape	plate
Radiation	MoK_α (λ=0.71073 Å)
2θ range [°]	3.89 to 52.04 (0.81 Å)
Index ranges	−29 ≤ h ≤ 29 −29 ≤ k ≤ 29 −25 ≤ l ≤ 25
Reflections collected	270041
Independent reflections	12302 R_{int} = 0.0517 R_{sigma} = 0.0190
Completeness to θ = 25.242°	99.9
Data / Restraints / Parameters	12302 / 2568 / 706
Goodness-of-fit on F^2	1.036
Final *R* indexes [I≥2σ(I)]	R_1 = 0.0872 wR_2 = 0.2334
Final *R* indexes [all data]	R_1 = 0.1183 wR_2 = 0.2738
Largest peak/hole [eÅ^{-3}]	5.42/−2.55

Packing of $Ag_8(L^{Br2})_2(PF_6)$

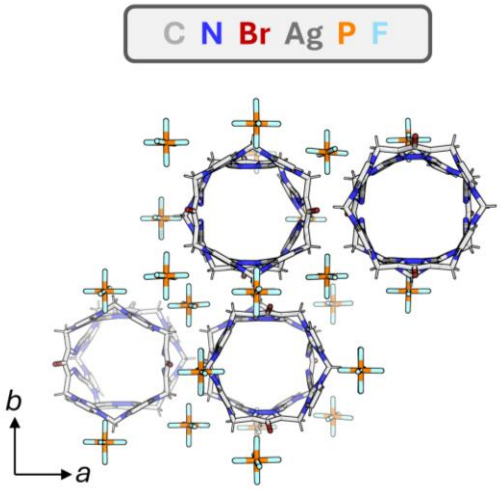

Figure S48: Graphical illustration of the packing of $Ag_8(L^{Br2})_2(PF_6)_4$ in the crystallographic c-axis. Solvent molecules and disorders are omitted for clarity.

Distance Measurements of $Ag_8(L^{Br2})_2(PF_6)$

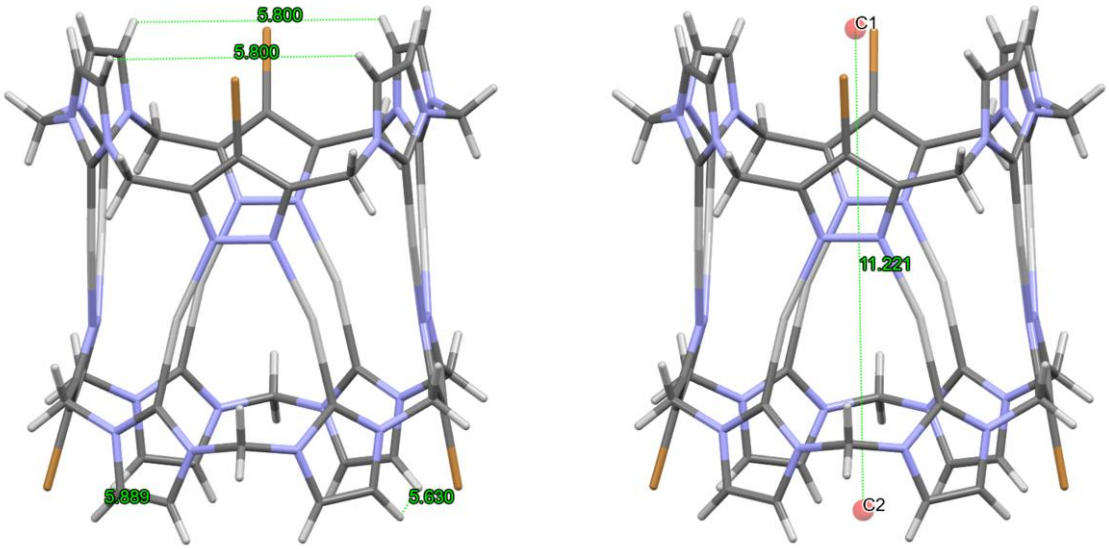

Figure S49: Calculation method for the portal opening of the pillarplex **$Ag_8(L^{Br2})_2(PF_6)_4$**: average distance of the outermost backbone protons minus 2x covalence radius of hydrogen (0.31 Å), Calculation method for the height of the pillarplex **$Ag_8(L^{Br2})_2(PF_6)_4$**: distance between two centroids defined by all backbone NHC protons of the rim. Hydrogen atoms are shown in the ideal calculated positions. Solvent molecules and counterions are omitted for clarity.

12.3 Compound $Au_8(L^{Br2})_2(PF_6)_4$ (2374513)

SC-XRD structure report for compound $Au_8(L^{Br2})_2(PF_6)_4$.

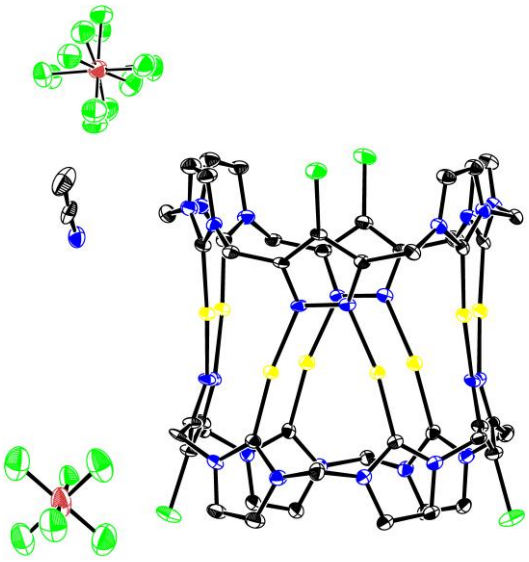

Figure S50: ORTEP representation of the solid-state structure of **$Au_8(L^{Br2})_2(PF_6)_4$** (C = black, N = blue, P = red, F = light green, Br = green and Au = yellow) shown with 50 % probability displacement ellipsoids. Two counterions are omitted for clarity.

A colourless, fragment-shaped crystal of $C_{52}H_{46}Au_8Br_4F_{24}N_{26}P_4$ coated with perfluorinated ether and fixed on top of a Kapton micro sampler was used for X-ray crystallographic analysis. The X-ray intensity data were collected at 123(2) K on a Bruker D8 VENTURE three-angle diffractometer with a TXS rotating anode with MoK_α radiation (λ=0.71073 Å) using APEX4.[16] The diffractometer was equipped with a Helios optic monochromator, a Bruker PHOTON III detector, and an Oxford Cryostreamlow temperature device.

A matrix scan was used to determine the initial lattice parameters. All data were integrated with the Bruker SAINT V8.40A software package using a narrow-frame algorithm and the reflections were corrected for Lorentz and polarisation effects, scan speed, and background.[17] The integration of the data using a tetragonal unit cell yielded a total of 231404 reflections within a 2θ range [°] of 4.01 to 51.52 (0.82 Å), of which 10144 were independent. Data were corrected for absorption effects including odd and even ordered spherical harmonics by the multi-scan method (TWINABS 2012/1).[31, 32] Space group assignment was based upon systematic absences, E statistics, and successful refinement of the structure.

The structure was solved by direct methods using SHELXT and refined by full-matrix least-squares methods against F^2 by minimising $\Sigma w(F_o^2 - F_c^2)^2$ using SHELXL in conjunction with SHELXLE.[20, 21, 22] All non-hydrogen atoms were refined with anisotropic displacement parameters. Hydrogen atoms were refined isotropically on calculated positions using a riding model with their U_{iso} values constrained to 1.5 times the U_{eq} of their pivot atoms for terminal sp^3 carbon atoms and a C–H distance of 0.98 Å. Non-methyl hydrogen atoms were refined using a riding model with methylene, aromatic, and other C–H

distances of 0.99 Å, 0.95 Å, and 1.00 Å, respectively, and U_{iso} values constrained to 1.2 times the U_{eq} of their pivot atoms.

Neutral atom scattering factors for all atoms and anomalous dispersion corrections for the non-hydrogen atoms were taken from International Tables for Crystallography.[29] Supplementary crystallographic data reported in this paper have been deposited with the Cambridge Crystallographic Data Centre (2374513) and can be obtained free of charge from The Cambridge Crystallographic Data Centre via www.ccdc.cam.ac.uk/structures.[24] This report and the CIF file were generated using FinalCif.[30] Images of the crystal structure were generated with *MERCURY*, *PLATON* and *PyMOL*.[25, 26, 27, 28]

Table S6: Crystal data and structure refinement for compound $Au_8(L^{Br2})_2(PF_6)_4$.

CCDC number	2374513
Empirical formula	$C_{52}H_{46}Au_8Br_4F_{24}N_{26}P_4$
Formula weight	3510.40
Temperature [K]	123(2)
Crystal system	tetragonal
Space group (number)	$P4_12_12$ (92)
a [Å]	14.3499(8)
b [Å]	14.3499(8)
c [Å]	51.556(4)
α [°]	90
β [°]	90
γ [°]	90
Volume [Å^3]	10616.4(14)
Z	4
ρ_{calc} [gcm^{-3}]	2.196
μ [mm^{-1}]	12.660
F(000)	6352
Crystal size [mm^3]	0.029×0.057×0.130
Crystal colour	colourless
Crystal shape	fragment
Radiation	MoK_α (λ=0.71073 Å)
2θ range [°]	4.01 to 51.52 (0.82 Å)
Index ranges	−17 ≤ h ≤ 17 −17 ≤ k ≤ 17 −62 ≤ l ≤ 62
Reflections collected	231404
Independent reflections	10144 R_{int} = 0.0666 R_{sigma} = 0.0229
Completeness to θ = 25.242°	99.9
Data / Restraints / Parameters	10144 / 1354 / 599
Goodness-of-fit on F^2	1.188
Final *R* indexes [I≥2σ(I)]	R_1 = 0.0483 wR_2 = 0.1080
Final *R* indexes [all data]	R_1 = 0.0551 wR_2 = 0.1116
Largest peak/hole [eÅ^{-3}]	2.20/−2.23
Flack X parameter	0.50(2)

Packing of $Au_8(L^{Br2})_2(PF_6)$

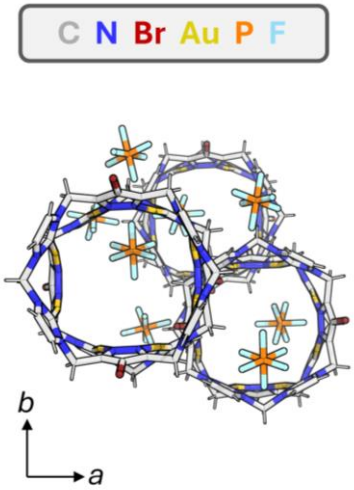

Figure S51: Graphical illustration of the packing of $Au_8(L^{Br2})_2(PF_6)_4$ in the crystallographic c-axis. Solvent molecules and disorders are omitted for clarity.

Distance Measurements of $Au_8(L^{Br2})_2(PF_6)$

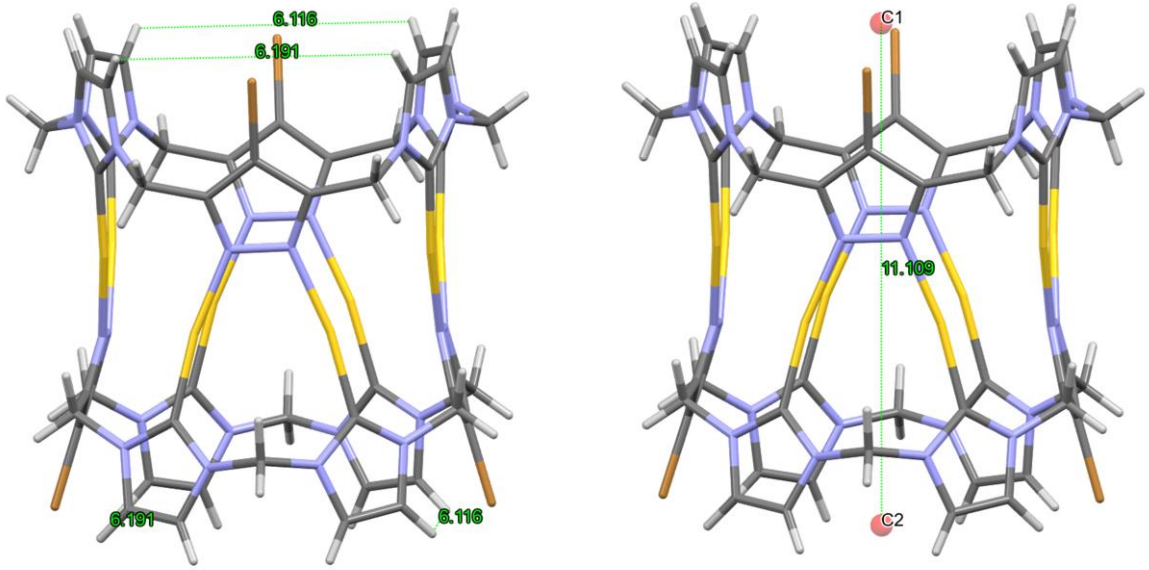

Figure S52: Calculation method for the portal opening of the pillarplex **$Au_8(L^{Br2})_2(PF_6)_4$**: average distance of the outermost backbone protons minus 2x covalence radius of hydrogen (0.31 Å), Calculation method for the height of the pillarplex **$Au_8(L^{Br2})_2(PF_6)_4$**: distance between two centroids defined by all backbone NHC protons of the rim. Hydrogen atoms are shown in the ideal calculated positions. Solvent molecules and counterions are omitted for clarity.

13. References

[1] M. Loos, C. Gerber, F. Corona, J. Hollender, H. Singer, *Anal. Chem.*, 2015, **87**, 5738.

[2] F. Neese, *Wiley Interdiscip. Rev. Comput. Mol. Sci.*, 2012, **2**, 73–78. http://dx.doi.org/10.1002/wcms.81.

[3] F. Neese, Software update: *The ORCA program system—Version 5.0., Wiley Interdiscip. Rev. Comput. Mol. Sci.*, 2022, **12**. https://doi.org/10.1002/wcms.1606.

[4] C. Adamo and V. Barone, *J. Chem. Phys*.,1999, **110**, 6158-69. https://doi.org/10.1063/1.478522.

[5] F. Weigend and R. Ahlrichs, *Phys. Chem. Chem. Phys*., 2005, **7**, 3297.

[6] D. Andrae, U. Haeussermann, M. Dolg, H. Stoll, H. Preuss, *Theor. Chim. Acta*, 1990, **77**, 123-141.

[7] S. Grimme, S. Ehrlich, L. Goerigk, *J. Comput. Chem*., 2011, **32**, 1456–1465.

[8] S. Grimme, J. Antony, S. Ehrlich and H. Krieg, *J. Chem. Phys.*,2010, **132**, 154104.

[9] Y.-S. Lin, G.-D. Li, S.-P. Mao, and J.-D. Chai, *J. Chem. Theory Comput*., 2013, **9**, 263−272. https://doi.org/10.1021/ct300715s.

[10] J.-D. Chai and M. Head-Gordon, *Phys. Chem. Chem. Phys.,* 2008, **10**, 6615–6620.

[11] J.-D. Chai and M. Head-Gordon, *J. Chem. Phys.*, 2008, **128**, 084106.

[12] F. Weigend, *Phys. Chem. Chem. Phys.*, 2006, **8**, 1057.

[13] S. Guan, T. Pickl, C. Jandl, L. Schuchmann, X. Zhou, P. J. Altmann and A. Pöthig, *Org. Chem. Front.*, 2021, **8**, 4061-4070.

[14] S.-Z. Hu, Z.-H. Zhou and B. E. Robertson, *Z. Kristallogr. – Cryst. Mater.*, 2009, **224**, 375-383.

[15] *ELDIX Software Suite*, Version 4.3.1; ELDICO Scientific AG: Villigen, Switzerland, 2023.

[16] *APEX4 Suite of Crystallographic Software, Version 2021-10.0,* Bruker AXS Inc., Madison, Wisconsin, USA, 2021.

[17] Bruker, *SAINT*, *V8.40B*, Bruker AXS Inc., Madison, Wisconsin, USA.

[18] Bruker, *SADABS*, Version 2016/2; Bruker AXS Inc.: Madison, WI, USA, 2016.

[19] L. Krause, R. Herbst-Irmer, G. M. Sheldrick, D. Stalke, *J. Appl. Cryst.,* 2015, **48**, 3–10, doi:10.1107/S1600576714022985.

[20] C. B. Huebschle, G. M. Sheldrick, B. Dittrich, *J. Appl. Cryst.,* 2011, **44**, 1281–1284, doi:10.1107/S0021889811043202.

[21] Sheldrick, G. M., *Acta Crystallogr*., *Sect. A* 2008, **64**, 112–122. https://doi.org/10.1107/S2053273314026370.

[22] Sheldrick, G. M., *Acta Crystallogr*., *Sect. C,* 2015, **71**, 3–8. https://doi.org/10.1107/S2053229614024218.

[23] Peng, L.-M., *Micron*, 1999, **54**, 481–485. https://doi.org/10.1107/S0108767398001901.

[24] C. R. Groom, I. J. Bruno, M. P. Lightfoot, S. C. Ward, *Acta Cryst.,* 2016, **B72**, 171–179, doi:10.1107/S2052520616003954.

[25] A. L. Spek, *Acta Crystallogr. D*, 2009, **65**, 148.

[26] C. F. Macrae, I. J. Bruno, J. A. Chisholm, P. R. Edgington, P. McCabe, E. Pidcock, L. Rodriguez-Monge, R. Taylor, J. van de Streek, P. A. Wood, *J. Appl. Crystallogr.,* 2008, **41**, 466.

[27] The PyMOL Molecular Graphics System, Version 2.5.4 Schrödinger, LLC, 2021.

[28] The AxPyMOL Molecular Graphics Plugin for PowerPoint, Version 2.5.4 Schrödinger, LLC, 2021.

[29] Ed. E. Prince, *International Tables for Crystallography Volume C, Mathematical, Physical and Chemical Tables*, International Union of Crystallography, Chester, England, 2006, 500–502; 219–222; 193–199.
[30] D. Kratzert, *FinalCif*, *V139*, https://dkratzert.de/finalcif.html.
[31] Bruker, *TWINABS* (version 2012/1), Bruker AXS Inc., Madison, Wisconsin, USA, 2012.
[32] Sevvana, M., Ruf, M., Usón, I., Sheldrick, G. M. & Herbst-Irmer, R., *Acta Cryst.*, **D75**, 1040-1050.